Int J Earth Sci (Geol Rundsch) (2018) 107:1127–1151
DOI 10.1007/s00531-017-1548-8

ORIGINAL PAPER

Geochemical and isotopic constraints on the role of juvenile crust and magma mixing in the UDMA magmatism, Iran: evidence from mafic microgranular enclaves and cogenetic granitoids in the Zafarghand igneous complex

Fatemeh Sarjoughian[1] · David Lentz[2] · Ali Kananian[3] · Songjian Ao[4] · Wenjiao Xiao[4]

Received: 8 February 2017 / Accepted: 15 October 2017 / Published online: 30 October 2017

Abstract The Zafarghand Igneous Complex is composed of granite, granodiorite, diorite, and gabbro that contain many mafic microgranular enclaves. This complex was emplaced during the late Oligocene (24.6 Ma) to form part of the Urumieh–Dokhtar magmatic arc of Central Iran. The enclaves have spheroidal to elongated/lenticular shapes and are quenched mafic melts in felsic host magma as evidenced by fine-grained sinuous margins and (or) locally transitional and diffuse contacts with the host rocks, as well as having disequilibrium textures. These textures including oscillatory zoning with resorption surfaces on plagioclase, feldspar megacrysts with poikilitic and anti-rapakivi textures, mafic clots, acicular apatites, and small lath-shaped plagioclase in larger plagioclase crystals all indicate that the enclaves crystallized from mafic magma that was injected into and mixing/mingling with the host felsic magma. The studied rocks have calc-alkaline, metaluminous compositions, with an arc affinity. They are enriched in large ion lithophile elements, light rare-earth elements, and depleted in high field strength elements with significant negative Eu anomalies. The Sr–Nd isotopic data for all of the samples are similar and display ISr = 0.705123–0.705950 and εNd (24.6 Ma) = − 1.04–1.03 with TDM ~ 0.9–1.1 Ga. The host granites and enclaves are of mixed/mingled origin and most probably formed by the interaction between the juvenile lower crust with a basaltic composition and old lower or middle continental crust as a major component and lithospheric mantle as a minor component; this was followed by fractional crystallization and possibly minor crustal assimilation. The source seems to be comprised of about 90–80% of the basaltic magma and about 10–20% of lower/middle-crust-derived magma. Geochemical characteristics indicate that the intrusion of these rocks from a subduction zone setting below the Central Iran micro-continent was related to an active continental margin, although was transitional to a transtensional setting possibly due oblique convergence to slab rollback or break-off.

Keywords Granitoids · Enclaves · Juvenile crust · Subduction · UDMA · Iran

Introduction

Granitoid rocks are the main components of the continental crust and are one of the keys to understanding the tectonic environment and overall geological evolution. They form from granitic melts that are often not primary melts, but are modified by various differentiation processes prior to emplacement and final crystallization. Granitoids are present in almost every continental geological setting, where the continental crust has been thickened by orogeny either during subduction and (or) collision. The genetic classification of granitoids is based upon the amount of crustal, mantle, or mixed components involved during their genesis (Barbarin and Didier 1992; Chappell 1999, 2004; Chen et al. 2002; Kaygusuz et al. 2014). Magma mixing or mingling could have taken place in a magma chamber and (or) in a

✉ Fatemeh Sarjoughian
Fsarjoughian2@gmail.com

[1] Department of Earth Sciences, Faculty of Sciences, University of Kurdistan, Sanandaj, Iran

[2] Department of Earth Sciences, University of New Brunswick, Fredericton NB E3B 5A3, Canada

[3] Department of Geology, University College of Sciences, University of Tehran, Tehran, Iran

[4] State Key Laboratory of Lithospheric Evolution, Institute of Geology and Geophysics, Chinese Academy of Sciences, Beijing 100029, China

conduit. While magma ascent through the crust changes its composition by both assimilation and fractional crystallization (AFC) processes, mixing with other magmas can result in the formation of mafic magmatic enclaves (MME) (e.g., Blundy and Sparks 1992; Geshi 2000; Barbarin 2005).

MMEs encompass a broad range of textures, structures, and compositions. They are characterized according to their structural relationship to the host rocks, although some of them are interpreted as xenoliths, restite, and autoliths. Xenoliths are foreign lithic fragments, usually country rock that were incorporated during emplacement and (or) crystallization of the host magma (e.g., Domenick et al. 1983; Bacon 1986). Xenoliths often have magmatic reaction textures. In contrast, restite components are considered to represent pods of the original refractory source material of the host granite that did not reach a critical melt fraction during differentiation (e.g., White and Chappell 1977; Chappell and White 1991). Autoliths are interpreted to represent accumulations of early formed, genetically related crystals that were trapped within its own residual liquid (e.g., Fershtater and Borodina 1977; Schonenberger et al. 2006). MME are widely accepted by many petrologists as evidence of an important process of generating hybrid magmas (e.g., Eichelberger 1975; Vernon 1984; Frost and Mahood 1987; Blundy and Sparks 1992; Poli et al. 1996; Perugini et al. 2003; Barbarin 2005; Sarjoughian et al. 2012). MMEs are dark fine-grained, rounded to elongate inclusions that are common within intermediate to felsic igneous rocks. Field, petrographic, and geochemical evidences for chemical (magma mixing) and physical (magma mingling) interactions between compositionally distinct magmas have been documented in many locations (e.g., Waight et al. 2000). Although some researchers (Laumonier et al. 2014a) believed that a purely physical mixing (magma mingling) never occurs as chemical diffusion will always proceed to some extent, depending on temperature and time lapse after the onset of contact between end-members. The physical and chemical processes that occur when a relatively hot mafic magma interacts with relatively cool felsic magma include the more mafic magma initially being thermally quenched and partially crystallize as it rapidly cools to thermal equilibrium with the felsic magma (Vernon 1990; Waight et al. 2000). During the approach to thermal equilibrium, changes in enclave viscosity occur with important consequences for the physical and chemical transfers of material between the MME and the host magma (Sparks and Marshall 1986). Disaggregation of an enclave will be controlled by the viscosity contrast and is unlikely to occur if the mafic blob has a viscosity higher by >0.3 log units relative to that of its host (Laumonier et al. 2014b). The viscosity contrast largely controls magma hybridization (Campbell and Turner 1986; Piochi et al. 1999). The viscosity of the MMEs increases due to evolution of the residual melt during crystallization and liquid–liquid exchange with the felsic melt (Sparks and Marshall 1986; Poli and Tommasini 1990). After attaining thermal equilibrium, the two magma components [one predominantly solid (MME) and the other liquid + crystals] then cool at the same slow rate and the residual MME melt (if present) continues to undergo both elemental and isotopic exchange with its host (Waight et al. 2000). Advocates of magma mixing explain the compositional similarities between enclaves and host rocks are due to varying degrees of chemical equilibration and diffusional exchange between the coexisting melt during slow cooling (Pin et al. 1990; Holden et al. 1991).

Granitoid rocks are an important characteristic component of the continental crust, and examining enclaves can be a powerful tool in investigating the evolution of those granitoid bodies. In addition, the petrogenesis of the Zafarghand igneous complex (ZIC) in the Urumieh–Dokhtar magmatic arc (UDMA) is still poorly understood and sources of their magmas remain unclear in detail. The geologic importance of the ZIC is to understand the geodynamic evolution of this area in regards to the final stages of the Neotethys subduction. On the other hand, many intrusions of the UDMA are not well studied; detailed research of individual igneous rocks can be a more appropriate approach to providing the kind of information required.

Therefore, in this paper, we present field relationships and textural characteristics, major- and trace-element geochemistry, and Sr–Nd isotopic data in the central part of the UDMA; the main purposes include: (1) describing the field studies, mineralogical composition, textural, and geochemical variations of the whole-rock units; (2) examining the magmatic evolution, by testing whether these mafic and felsic rocks are cogenetic, and to investigate the magmatic fractionation and magma mixing/mingling processes between these various rocks; (3) discussing its dominant tectonic process and regional geodynamic regime during magmatism; (4) constraints on their source characteristics and petrogenesis; (5) developing an understanding of the relationship between the petrogenetic processes and the geodynamic setting of this region; and (6) examining these data to compare with previously studied intrusive rocks in the UDMA and other granitoids from similar geochemical contexts.

The new petrological data provide a revised petrogenetic scenario for arc-related magmatism leading to a better understanding of the complex evolution of the UDMA in this part of the Neotethys orogen. The Nd–Sr isotopic compositions of the ZIC support their relatively juvenile character, which implies a crustal growth in the Paleo to NeoProterozoic.

Regional geology

The Zagros orogen, a member of the Alpine–Himalayan orogenic belt, formed from the collision of Eurasia with dispersed fragments of Gondwana (e.g., Berberian and King 1981; Alavi 1994; Agard et al. 2005; Ao et al. 2016). According to regional tectonics, magmatic sequences, paleogeography, and ophiolite remnants from the Late Precambrian until Late Paleozoic, Gondwana was separated from the Eurasian plate by the Variscan ocean called Paleotethys. During the Middle-to-Late Triassic, coeval with the closure of the Paleotethys in the north, a rifting episode along the Zagros belt resulted in the opening of a new ocean called Neotethys. Final closure of Paleotethys is a consequence of the subduction of the oceanic crust of the Neotethys beneath the Eurasian plate (Berberian and Berberian 1981).

The NW-trending Zagros mountains represent one of the youngest continental collision zones on Earth. The Zagros Orogen has been divided into the external Zagros Fold and Thrust Belt and the internal Sanandaj–Sirjan zone that flanked by the Tertiary UDMA. The ~2000 km-long and 150 km-wide UDMA is an Andean-type Cordilleran magmatic arc system and forms a subduction-related, voluminous magmatic arc composed of tholeiitic, calc-alkaline, and K-rich alkaline intrusive and extrusive rocks (Berberian and King 1981; Omrani et al. 2008). There is a general agreement that subduction and arc magmatism began in latest Triassic/Early Jurassic time (Hassanzadeh and Wernicke 2016), but the time of the continental collision between Arabia and Eurasia is still controversial. The timing of collision between Arabia and Eurasia has long been a subject of debate, which include: (1) ophiolite obduction in the Late Cretaceous and coeval development of a foreland basin on the Arabian margin (Berberian and King 1981; Alavi and Mahdavi 1994); (2) an Eocene foreland basin in the Zagros and Eocene angular unconformities in Central Iran (Hempton 1987; Beydoun et al. 1992); (3) Late Eocene based on structural, lithological, and palaeobiogeographical evidences from both sides of the original Arabia–Eurasia suture (Allen and Armstrong 2008; Allen 2009); (4) Early-to-Mid-Miocene transition from marine to non-marine sedimentation (McQuarrie et al. 2003); (5) Early Miocene based on the deformation and syn-tectonic sedimentation that took place on the northern side of the Arabian plate (Robertson 2000); and (6) Miocene age of collision between Arabia and Eurasia, based on the imbrication and development of blind thrusting and folding in the Zagros Fold–Thrust Belt (Mohajjel et al. 2003).

It has also been suggested that collision between the Arabian and Iranian continental plates was diachronous along the Zagros suture zone. Agard et al. (2005) suggested that collision started prior to 25–23 Ma in northern Zagros Mountains and resulted in 70 km of shortening over the last 20–15 Ma alone within the Zagros Mountains south of the Main Zagros Thrust and northwest of the Thrusted Zagros (Whitechurch et al. 2013). Agard et al. (2011) proposed that the collision in the NW part of the suture started from 30 Ma, whereas in the SE part happened from 20 Ma.

It also seems likely that the collision was initially relatively "soft" (Ballato et al. 2011), perhaps beginning in the Eocene (e.g., Allen and Armstrong 2008), with final "hard" collision occurring in the late Oligocene or early middle Miocene (Karagaranbafghi et al. 2012; McQuarrie and van Hinsbergen 2013; Ali et al. 2013). Some new studies (e.g., Hooper et al. 1994; Hafkenscheid et al. 2006; Robertson et al. 2009; Chiu et al. 2013; Richards 2015) show that collision happened diachronously from early Miocene in the northwest of Iran to late Miocene in the southeast. Mohajjel and Fergusson (2014) also believed that continental collision was initiated in the Oligocene, but the Tethyan seaway remained open until the mid-Miocene. Hatzfeld and Molnar (2010) suggested that collision in the Zagros seems to have begun between ~ 35 and ~ 23 Ma as well across the orogen.

Moreover, Ao et al. (2016) indicate that the final closure of the Neotethys Ocean occurred in the Late Miocene, based on the Kermanshah ophiolite that was probably an ancient oceanic core produced by large oceanic detachment faults.

The ZIC is located in Central UDMA that tried to identify a major tectonic regime in these fields. Moreover, the geochemistry of many intrusions of the UDMA is not well known, and only a few intrusive rocks, such as Khalkhab–Neshveh (Rezaei-Kahkhaei et al. 2011); Ghalhar, Marfion, and Poudalg (Honarmand et al. 2014); Natanz (Haschke et al. 2010); Kajan (Golkaram et al. 2016); Kuh-e Dom (Kananian et al. 2014); Kal-e-Kafi (Ahmadian et al. 2016); and Kuh Panj and Jebal Barez (Shafiei et al. 2009; Asadi et al. 2014) were examined in detail. We, therefore, conclude that the entire geological history of the magmatic arc in the Zagros orogenic belt is still relatively not well understood.

Field relations

The ZIC is located 40 km south of Ardestan in Central UDMA and exhibits an elongated northeast–southwest shape. The studied complex is situated between the latitudes of 33°00′N and 33°12′N and the longitudes of 52°18′E and 52°30′E in the UDMA and covers an outcrop area of ~ 80 km^2. The surrounding rocks of the ZIC are dominated by successions of Eocene basalt, andesite, latite, dacite, rhyolite, tuff, and ignimbrite. The contacts between the pluton and volcanic rocks are predominantly sharp and discordant. The volcanic rocks are metamorphosed near their contacts with the plutonic bodies and the grade of contact metamorphism is locally within the albite–epidote hornfels to hornblende hornfels facies (Fig. 1).

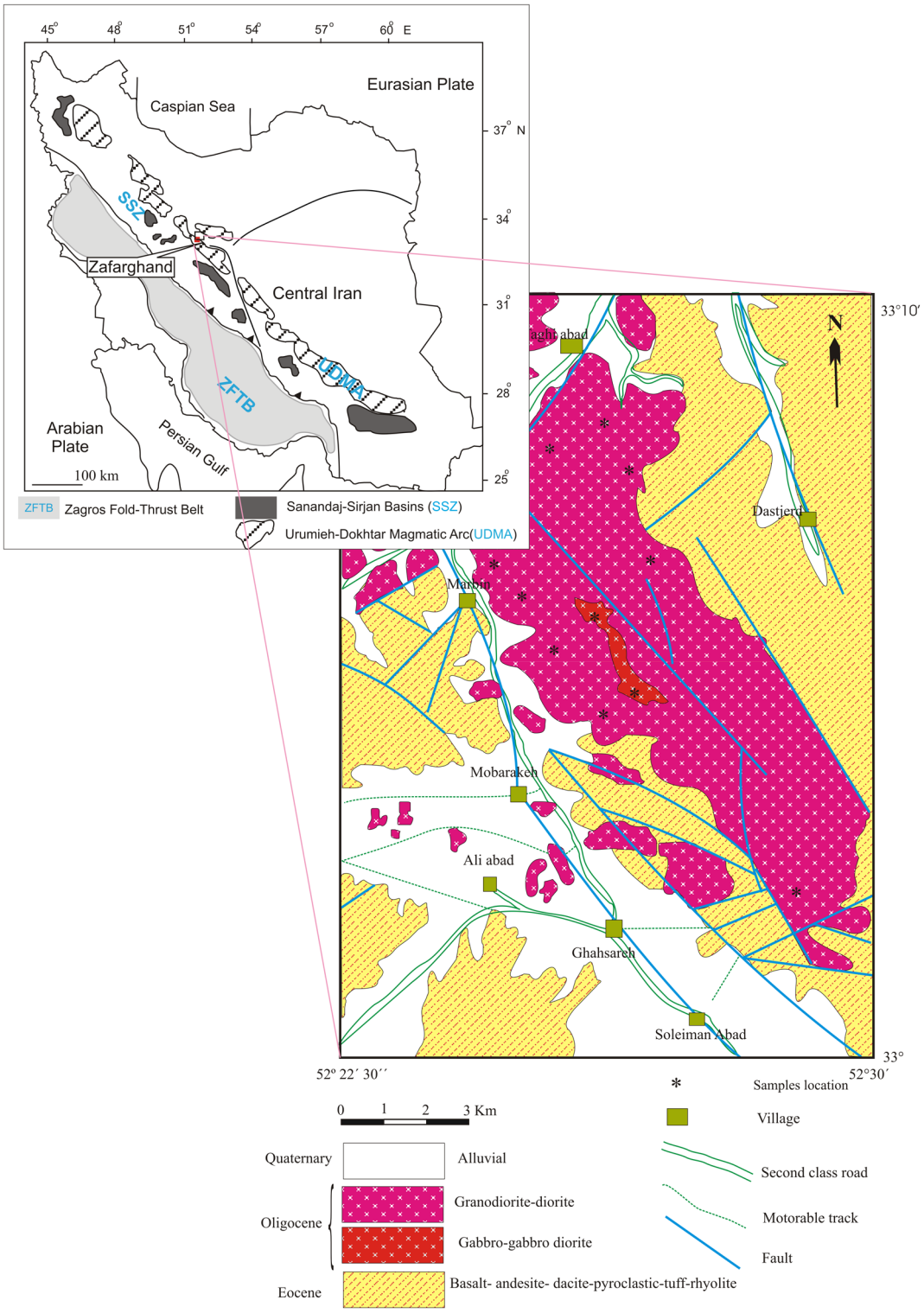

Fig. 1 Simplified geological map of the Zafarghand complex (Iran), based on Radfar et al. (1999; slightly modified)

The textural evidence, such as local granophyric textures, sharp and angular contacts, medium-to-low-grade thermal metamorphic aureole, and hydrothermal alteration, indicate a shallow depth of emplacement of the studied rocks, where crystallization pressures should be <2 kbar (see Clarke 1992).

The ZIC ranges in composition from gabbro to granite. The interior portions of the pluton range in composition from gabbro, diorite, and granodiorite and to granite in the north. The granodiorite is a transitional rock between these two zones. In the southeastern part, the zoned rocks are classified as diorite and granodiorite, and in the northwestern part, the rocks are mostly granodiorite. The diorites and granodiorites are dark to light grey in colour and have a fine-to-coarse-grained texture. The gabbro is poorly exposed within the centre of the elliptically shaped pluton; they are coarse to medium grained and black to dark grey in colour. Internal contacts between all these bodies are gradational, but the gabbro usually has sharp contacts with the granodiorites and diorite. The granites are light cream to white in colour, generally fine-grained, and have granular to porphyritic textures with megacrysts of feldspar; they are mostly exposed in the northern and northwestern parts of the complex. The age of the granodioritic rocks was determined to be 24.6 ± 1.0 Ma by U–Pb zircon dating (Sarjoughian and Kananian 2017).

MMEs are common in the granodiorite rocks with semi-rounded, elongate, and irregularly shapes and are centimetres to metres in size (Fig. 2a) and their modal mineralogy ranges from gabbro to diorite. In some places, MMEs display sharp contacts with host rocks, whereas elsewhere, the contacts between the enclaves and the surrounding host are gradational and locally diffuse and mingling–mixing features of enclave magmas are common (Fig. 2b). This interface is marked by a variety of hybridization textures including ellipsoid/lobate MME with chilled margins, feldspar megacrysts in MME (Fig. 2c), and crenulated margins in enclaves. Some enclaves show spalling and net veining by the host granitic magma. Collectively, mingling/mixing phenomena between mafic and felsic magmas are convincing evidence that they were mostly liquids at the time.

This complex is crosscut by late-stage, NE–SW and E–W trending porphyritic microgranite, microgranodiorite, and aplite dykes, ranging in thickness from a few cm to 1 m; chilled margins are not evident. Some doleritic dykes with andesitic compositions show embossed shape in the area, suggesting incomplete solidification of the host during dyke emplacement. Elsewhere, repetitively layered, mafic pillows in a host rock indicate the operation of successive cycles of injection, chilling, and sinking of mafic magma into a pre-existing felsic magma chamber. These features suggest that perhaps, dykes and intrusion magmas coexisted and mingled (e.g., Keay et al. 1997).

Petrography

The ZIC mainly consists of granodiorite, diorite, and gabbro with lesser proportions of granite. These granodiorites contain plagioclase (28–45%), amphibole (4–9%), biotite (5–18%), K-feldspar (22–30%), and quartz (18–29%). Plagioclase shows oscillatory zoning and twinning. Plagioclase occurs both as small euhedral laths and as larger crystals. Plagioclase shows anti-rapakivi texture, mantled by orthoclase. Amphibole occurs as euhedral-to-subhedral crystals. Biotite is abundant in the granodiorites. It is subhedral and anhedral and forms prismatic crystals and lamellas. In addition, occurrence of clots of mafic and accessory minerals consists predominantly of hornblende crystals intergrown with biotite, titanite, and opaque minerals. K-feldspar forms anhedral, rarely subhedral crystals of perthitic orthoclase. Quartz is anhedral with irregular cracks and occurs interstitially to the other minerals. Zircon, apatite, titanite, and opaque minerals are the accessory phases. Secondary minerals mainly include epidote, chlorite, calcite, sericite, and clay minerals.

The dioritic rocks mainly consist of polysynthetic twinned and zoned plagioclase (42–66%) and prismatic amphibole (11–38%). Biotite (4–18%) occurs in the more evolved parts of these rocks. Minor quartz (0.2–3.5) and alkali feldspar (7–15%) with interstitial texture also occur. Plagioclase forms subhedral-to-anhedral and lath-shaped

Fig. 2 Field photographs of: **a** typical outcrop of mafic microgranular enclaves in the host rock. **b** Diffuse zone at contact with host rock. **c** Megacrysts of alkali feldspar in the contact enclave-host rock

crystals, which also contain small plagioclase and amphibole inclusions. Some plagioclase crystals are altered to sericite and clay minerals. Amphibole occurs as euhedral-to-subhedral prismatic crystals and is locally altered to actinolite, biotite, titanite, chlorite, and calcite. Clinopyroxene mostly forms subhedral crystals and is found less frequently than the other mafic minerals. It is locally partially altered to actinolite, epidote, and chlorite with titanite, apatite, zircon, and opaque minerals occurring as accessory phases.

The mineralogy of the gabbro is very similar to that of the diorites, containing more pyroxene (0.2–4.3%), plagioclase (48–63%), and amphibole (29–42%), with no biotite observed. Clinopyroxene is a primary mafic phase in the rock and some pyroxenes are replaced by actinolite, uralite, and calcite. Plagioclase occurs as zoned euhedral-to-subhedral laths and commonly shows oscillatory or normal concentric zoning with variable degrees of sericitization. Brown hornblende tends to be fine-grained, euhedral-to-subhedral crystals, which are corroded in some samples. Locally, K-feldspar (0–3%) and quartz (0–0.4%) occur as anhedral interstitial crystals. Accessory minerals include titanite, Fe–Ti oxides, and apatite. Secondary minerals include actinolite, epidote, chlorite, calcite, sericite, and clay minerals.

Granites consist of abundant euhedral-to-anhedral crystals of alkali feldspar (39–54%), plagioclase (12–26%), interstitial quartz (27–41%), biotite (3–4%), and rare amphibole (0–1.1%). Granites contain less than 5% mafic minerals, most of which is biotite and minor amphibole. Quartz and K-feldspar occur as groundmass subhedral-to-anhedral crystals. Accessory phases include apatite and zircon. Kaolinitization and sericitization of feldspar and chloritization of biotite were observed.

MMEs are fine-grained compared with the host rocks. They are gabbroic and dioritic and have similar mineralogical features as their host rocks, but contain more abundant hornblende (22–46%), plagioclase (31–66%), and slightly less abundant quartz (1.5–6%), K-feldspar (1–18%), and biotite (3–17%). The enclaves have a fine-grained granular texture, except in the larger enclaves. Towards the contact with the host rocks, the enclaves possess a fine-grained texture (about 0.1–0.2 mm); towards the centre of the pluton, medium-grained textures predominate (about 0.5–1.5 mm). Plagioclase occurs as zoned euhedral-to-subhedral laths and commonly shows oscillatory and normal concentric zoning and prismatic-cellular growth (Fig. 3a, b). Some large plagioclase crystals contain small plagioclase inclusions. Hornblende occurs as euhedral-to-subhedral grain shapes, and is of two generations with brown or green colours. Plagioclase phenocrysts and hornblende prisms occur across MME–host rock boundary. Quartz is anhedral in shape and fills interstices between other minerals. Two varieties of alkali feldspar were distinguished in the enclaves: one variety is megacrysts and the other is anhedral crystals, which are associated with quartz-forming poikilitic and interstitial aggregates. Large K-feldspar crystals with an identical size to phenocrysts in the host granites also occur inside the enclaves. Large K-feldspar phenocrysts have poikilitic textures, in which they often contain inclusions that include small crystals such as quartz, biotite, plagioclase, and opaque minerals (Fig. 3c). Large K-feldspar crystals commonly crosscut (straddle) the enclave/host boundary. Titanite, zircon, and opaque minerals are the other key accessory minerals.

Analytical methods

After petrographically characterizing the rock types, we took special care in the selection of the samples for analytical work by choosing the most representative samples from various lithologies in the ZIC. One hundred samples were collected for petrographic analysis. After petrographically characterizing the plutonic rock types, 11 representative samples with the least amount of alteration

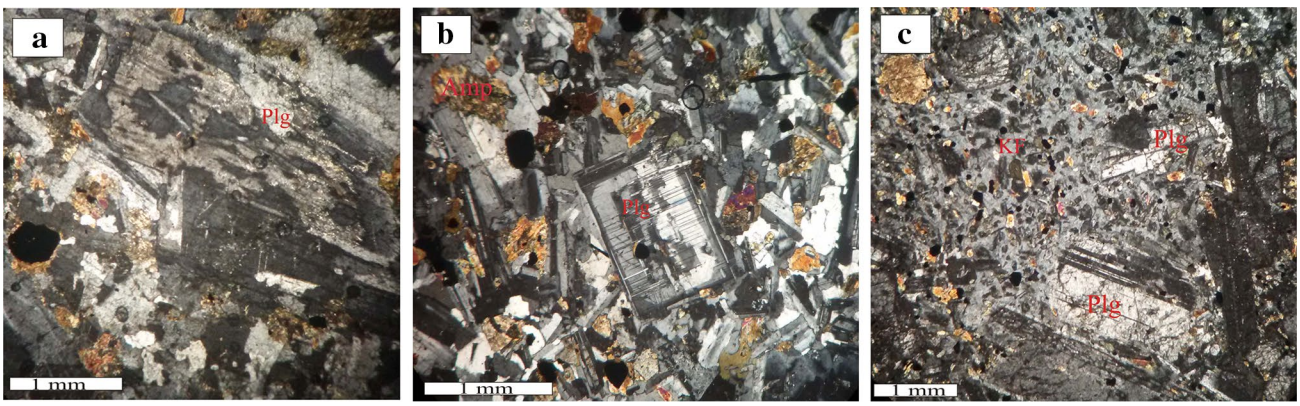

Fig. 3 **a, b** Plagioclase megacrysts with oscillatory zoning, **c**. K-feldspar megacryst with poikilitic texture. Cross-polarized transmitted light

were selected for whole-rock geochemical analysis by X-ray fluorescence (XRF) spectrometry, lithium metaborate fusion inductively coupled plasma-mass spectrometry (ICP-MS), and radiogenic tracer isotopic analysis (Rb–Sr and Sm–Nd). Whole-rock powders prepared with rock crushing in a steel jaw crusher, splitting, and pulping in a swing mill.

The major elements were analyzed by XRF (Rigaku RIX 2000 with Rh end window tube) using fused glass disks at Naruto University. Glass beads, from finely grounded samples, were prepared with sample to flux ($Li_2B_4O_7$) and analyzed for major elements using the fundamental parameter method spectrometry. Analytical errors are usually less than 1%.

Trace and REEs were analyzed using fusion ICP–MS at ALS Chemex Company in Canada. These elements were analyzed after fusion of 0.2 g of rock powder with 1.5 g $LiBO_2$ that were then dissolved in 100 mL 5% HNO_3. Detection limits range 0.1–10 ppm for trace elements and 0.01–0.5 ppm for REEs.

The Nd and Sr isotopic ratios were analyzed at the Institute of Geology and Geophysics, China (IGGCAS). These analyses followed procedures similar to those described by Li et al. (2012a) and Yang et al. (2010). Whole-rock powders for Sr and Nd isotopic analyses were dissolved in Savillex Teflon screw-top capsule after being spiked with the mixed ^{87}Rb–^{84}Sr and ^{149}Sm–^{150}Nd tracers prior to $HF + HNO_3 + HClO_4$ dissolution. Rubidium, Sr, Sm, and Nd were separated using the classical two-step ion exchange chromatographic method and measured using a Thermo Fisher Scientific Triton Plus multi-collector thermal ionization mass spectrometer at IGGCAS. The whole procedure blank was lower than 300 pg for Rb–Sr and 100 pg for Sm–Nd. The isotopic ratios were corrected for mass fractionation by normalizing to $^{88}Sr/^{86}Sr$=8.375209 and $^{146}Nd/^{144}Nd = 0.7219$, respectively. International standard samples, NBS-987 and JNdi-1, were also run to evaluate instrument stability during the period of data collection. The measured values for the NBS-987 Sr standard and JNdi-1 Nd standard were $^{87}Sr/^{86}Sr = 0.710250 \pm 0.000021$ ($n = 9$, 2 SD) and $^{143}Nd/^{144}Nd = 0.512118 \pm 0.000014$ ($n = 9$, 2 SD), respectively. USGS reference material BCR-2 was used to monitor the accuracy of the analytical procedures, with the following results: $^{87}Sr/^{86}Sr = 0.705028 \pm 0.000012$ and $^{143}Nd/^{144}Nd = 0.512635 \pm 0.000014$. The $^{87}Sr/^{86}Sr$ and $^{143}Nd/^{144}Nd$ data of BCR-2 are in good agreement with previously published data by TIMS and MC-ICP-MS techniques (Li et al. 2012a, b). The previous data on the host rocks from Sadeghian and Ghaffary (2011; major and trace elements) are also used.

Results

Major- and trace-element geochemistry

Major and trace, including rare-earth elements, contents of the ZIC are presented in Table 1. The analyses of the host granitoid samples of this study, and recently, reported data (Sadeghian and Ghaffary 2011) indicate that the ZIC has features typical of calc-alkalic, magnesian rocks with an I-type source affinity. In the de la Roche et al. (1980) classification scheme for plutonic rocks, the Zafarghand rocks plot as three main groups, the felsic rocks, mafic-intermediate rocks, and MMEs. The mafic-intermediate and MMEs plot mainly within the gabbro, gabbro-diorite, and diorite fields, whereas the felsic rock types mostly plot as a continuum in the granite to granodiorite fields (Fig. 4). Overall, the SiO_2 contents range from 52.01 to 77.56 wt%. However, the felsic and mafic-intermediate rocks display narrow variation intervals that do not overlap: 52.01–58.61 wt% SiO_2 for the mafic-intermediate suite and 65.38–77.56 wt% for the felsic rocks, but the enclaves overlap with the mafic-intermediate unit: 55.15–57.09 wt% SiO_2 for the enclaves. The A/CNK ratio [molecular $Al_2O_3/(CaO + K_2O + Na_2O)$] of the studied suite ranges from 0.68 to 1.01, and all samples are metaluminous (Maniar and Piccoli 1989). In the MALI ($Na_2O + K_2O - CaO$) vs. SiO_2 diagram (Frost et al. 2001; Fig. 5a), the data points lie in the calcic to calc-alkaline fields. Most of the samples plot in the field of calc-alkaline rocks using the Zr/Y vs. Th/Yb discrimination diagram (Ross and Bedard 2009; Fig. 5b). The felsic rocks have lower concentrations of Fe_2O_{3T}, Al_2O_3, MgO, TiO_2, and CaO relative to the mafic-intermediate rocks and MME. Trace elements are characterized by low Cr, Ni, and Sr, but high abundant of Zr and Nb and variable Rb and Ba (not shown).

Chondrite-normalized REE patterns (Sun and McDonough 1989) are shown in Fig. 6a. In this diagram, the pattern of rare elements in all units is similar with enrichment of light REE (LREEs) relative to heavy REEs (HREEs) (La_N/Yb_N: 1.9–5.9), approximately 10–100 times chondrite, and a flat HREE pattern (Gd_N/Lu_N: 1.07–1.41). Pronounced negative Eu anomalies to minor positive Eu anomalies (Eu_N/Eu^*) between 0.24 and 1.19 are present. The depletion of Eu is indicative of feldspar involvement during fractionation and (or) melting (cf. Rollinson 1993), whereas the lack of a significant negative Eu anomaly in some samples can indicate either: (1) lack of plagioclase fractionation from primitive magmas; (2) suppression of plagioclase fractionation due to high magmatic water contents; or (3) a high magmatic oxidation state that limits the replacement of Ca by Eu in plagioclase (Drake and Weill 1975; Hanson 1980). Positive Eu anomalies can also indicate either plagioclase accumulation in the rock or fractionation of hornblende, since under those conditions, the amphibole has typically a low partition

Table 1 Result of major oxides (wt%) and trace element (ppm) in the Zafarghand igneous complex

Felsic rocks					Mafic-intermediate rocks				Enclaves		
Sample	ZG1	ZG2	ZG3	ZG4	ZD1	ZD2	ZD3	ZD4	ZE1	ZE2	ZE3
Type	Granite	Granodiorite	Granite	Q-monzonite	Gabbro-diorite	Gabbro	Monzodiorite	Gabbro	Gabbro-diorite	Gabbro-diorite	Monzogabbro
SiO_2	77.56	73.72	75.93	65.38	54.29	52.01	58.61	52.25	55.15	56.48	57.09
TiO_2	0.11	0.55	0.33	0.72	1.26	1.51	0.88	1.04	1.18	0.79	1.13
Al_2O_3	12.14	13.52	13.01	15.30	17.94	15.79	16.38	16.55	17.10	17.53	16.96
Fe_2O_3	0.61	0.88	0.41	2.48	3.02	3.70	3.22	3.14	2.94	2.67	2.51
FeO	0.64	1.27	0.49	2.90	5.66	7.59	4.45	5.72	5.87	4.01	3.59
MnO	0.02	0.03	0.02	0.09	0.19	0.17	0.20	0.05	0.23	0.07	0.04
MgO	0.11	0.81	0.55	1.47	3.53	5.34	5.18	6.21	4.14	3.97	3.04
CaO	0.62	3.46	2.13	3.22	8.66	8.93	3.56	9.24	8.56	7.56	8.36
Na_2O	3.72	5.18	6.75	5.36	3.64	3.13	4.21	4.25	3.33	5.38	5.42
K_2O	4.39	0.35	0.24	2.53	0.79	0.71	2.57	0.54	0.55	0.81	1.16
P_2O_5	0.01	0.10	0.07	0.18	0.35	0.24	0.19	0.35	0.28	0.25	0.28
Total	99.93	99.87	99.93	99.64	99.33	99.12	99.45	99.33	99.33	99.52	99.58
Ni	*	1.9	2.4	*	11.9	47.5	8.1	54.9	25.7	35.7	9.6
Ba	1215	96.9	40.6	422	346.5	275	610	142.5	404	371	405
Cs	1.39	*	0.41	1.31	*	1.14	1.29	0.38	1.67	1.05	0.41
Ga	14.1	*	14.1	17.8	*	18.8	17.9	17.4	18.6	19	18.8
Hf	6.2	*	8	6.9	*	3	4.3	3	5.7	3.2	4.6
Nb	9.8	10.3	9.8	13.2	7.1	6.7	8.9	9.4	9.6	7.3	8.9
Rb	123.5	12.4	5.2	93.3	20.3	25.8	64.2	11.5	13.5	26.3	18.2
Sr	43.2	254.4	161.5	159	336.6	342	252	414	348	355	416
Ta	1	*	0.9	1.1	*	0.4	0.6	0.5	0.6	0.4	0.6
Th	15	19.3	14.55	12.5	3.7	2.67	8.04	1.55	3.96	2.38	3.14
La	27	*	12.4	26.2	*	12.7	22.3	16.2	20	19.3	16.6
Ce	58.9	48.8	41.4	61.3	34.1	28.6	46.3	34.2	43.8	42.1	39.1
Pr	7.23	*	6.03	8.06	*	3.93	5.67	4.29	5.77	5.44	5.25
Nd	26.6	*	23.7	31.9	*	16.7	21.4	16.9	23	21.2	21.3
Sm	6.07	*	6	7.89	*	4.4	4.65	3.88	5.68	4.82	5.43
Eu	0.51	*	0.47	1.04	*	1.35	1.2	1.1	1.39	1.73	1.52
Gd	5.91	*	5.99	8.54	*	4.97	4.57	4.11	6.04	4.74	5.78
Tb	1.07	*	1.08	1.49	*	0.85	0.7	0.64	1	0.79	0.94
Dy	6.82	*	7.07	9.69	*	5.32	4.4	3.94	6.3	4.78	5.99
Ho	1.52	*	1.53	2.14	*	1.13	0.93	0.85	1.32	1	1.28
Er	4.55	*	4.44	6.2	*	3.18	2.55	2.27	3.68	2.79	3.51

Table 1 (continued)

Felsic rocks					Mafic-intermediate rocks				Enclaves		
Sample	ZG1	ZG2	ZG3	ZG4	ZD1	ZD2	ZD3	ZD4	ZE1	ZE2	ZE3
Type	Granite	Granodiorite	Granite	Q-monzonite	Gabbro-diorite	Gabbro	Monzodiorite	Gabbro	Gabbro-diorite	Gabbro-diorite	Monzogabbro
Tm	0.75	*	0.69	0.99	*	0.47	0.39	0.35	0.57	0.44	0.55
Yb	5.04	*	4.35	6.25	*	3.01	2.54	2.18	3.58	2.79	3.41
Lu	0.81	*	0.64	0.99	*	0.49	0.4	0.36	0.58	0.44	0.56
U	3.72	*	2.5	3.6	*	0.69	1.68	0.41	1.1	0.82	0.78
V	4.5	*	23	84	*	478	222	210	320	185	210
Zr	170	303.5	270	240	158.1	110	160	120	240	130	180
Y	45.1	30.1	46.7	62.5	23.9	31.5	25.4	23.7	37.7	29.2	36.8
Pb	8.1	2.2	1.4	*	19.5	4	5.4	1.7	6.2	4.4	2.6
Cr	10	*	10	*	20.8	70	20	160	50	110	20

*not analysed

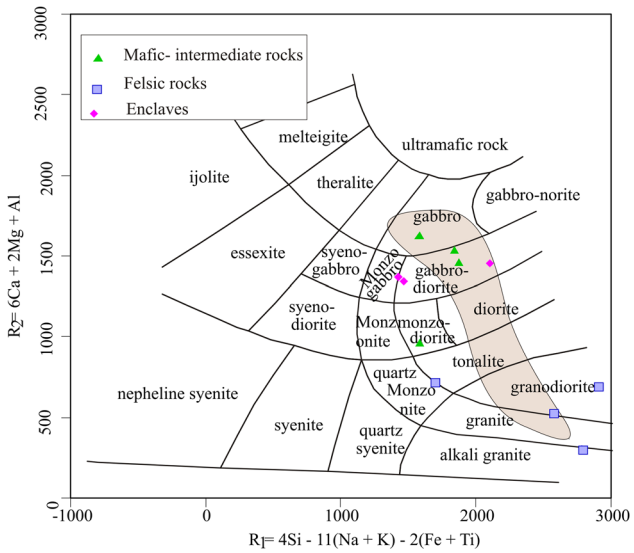

Fig. 4 R1–R2 compositional discrimination diagram (de la Roche et al. 1980) used for classification of the studied samples of the Zafarghand complex. Shaded field represents compositions of the Zafarghand complex (Sadeghian and Ghaffary 2011)

coefficient for Eu (e.g., Green and Pearson 1985; McKenzie and O'Nions 1991; Richards et al. 2012).

In the primitive mantle-normalized multi-element variation diagram (Fig. 6b; Sun and McDonough 1989), the felsic rocks, the mafic-intermediate rocks, and the MMEs are somewhat similar and all of samples are enriched in large ion lithophile elements (LILEs; e.g., Cs, Th, Rb, K, and Pb) and relatively depleted in high field strength elements (HFSEs; e.g., Nb, Ti, Y, and Yb). The enrichment in LILEs relative to HFSEs could have resulted from a low degree partial melting in mantle; the relative role of partial melting of metasomatized mantle and contamination by crustal materials is inferred in the formation of the region's rocks (e.g., Rogers et al. 1989; Sajona et al. 1996). The negative Nb and Ti anomalies also can indicate fractionation of a Ti-rich phase at their source (e.g., Çolakoğlu and Arehart 2010).

The granites also show negative Sr, Ba, and P anomalies, but the mafic-intermediate and MME have a varying Sr, Ba, and P anomalies with pronounced negative anomalies to minor positive anomalies. Negative Eu, Ba, and Sr anomalies imply feldspar separation during the differentiation or the presence of plagioclase in the source rocks. The ZIC display compositional trends consistent with fractional crystallization on Dy/Yb vs. Dy and La/Yb vs. La diagrams (Fig. 7a, b; Gao et al. 2007), suggesting that this process was responsible for their petrogenesis.

In addition, the plots of Rb/Sr vs. Sr (after Geng et al. 2009), and Sr vs. Rb (e.g., Osterhus et al. 2014) indicate that fractional crystallization of the plagioclase plays an important role in magmatic evolution (Fig. 8a, b). In Fig. 8c, all

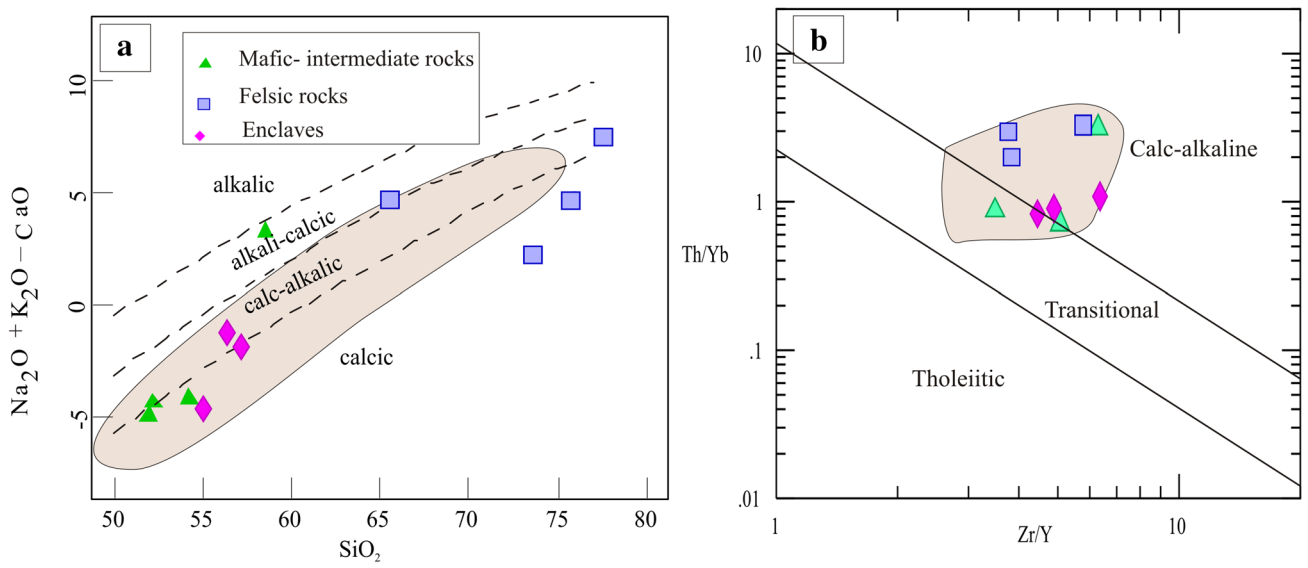

Fig. 5 **a** SiO_2 vs. $Na_2O + K_2O - CaO$ (Frost et al. 2001). **b** Zr/Y vs. Th/Yb (Ross and Bedard 2009) diagrams for discrimination of magmatic affinities. Shaded field represents compositions of the Zafarghand complex (Sadeghian and Ghaffary 2011)

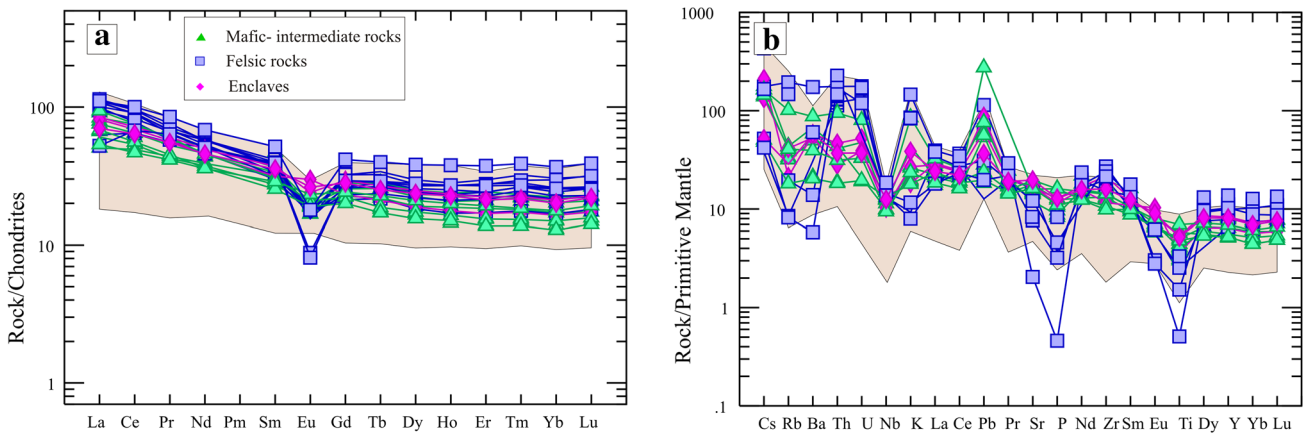

Fig. 6 **a** Chondrite-normalized REE patterns. **b** Primitive mantle-normalized trace-element compositions of the Zafarghand complex (normalization factors from Sun and McDonough 1989). Shaded field represents compositions of the Zafarghand complex (Sadeghian and Ghaffary 2011)

the samples show trends of decreasing Dy/Yb with increasing SiO_2. These trends show that amphibole and plagioclase fractionation have played an important role in magma genesis, because amphibole fractionation (KdMREE > KdHREE) will decrease Dy/Yb ratios (Davidson et al. 2007; Macpherson et al. 2006; Macpherson 2008). Moreover, the negative P anomalies result from apatite fractionation.

Sr–Nd isotopic composition

The Rb–Sr and Sm–Nd isotope data were determined for eight whole-rock samples and are presented in Table 2 and illustrated in Fig. 9. The initial $(^{87}Sr/^{86}Sr)_i$ and $(^{143}Nd/^{144}Nd)_t$ have been calculated at the U–Pb zircon age of 24.6 Ma (Sarjoughian and Kananian 2017) and all samples are assumed to be coeval. The samples mostly plot in the right quadrants of a conventional Sr–Nd isotope diagram and show a negative correlation between $(^{143}Nd/^{144}Nd)_t$ and $(^{87}Sr/^{86}Sr)_i$ values. The felsic rocks show $(^{87}Sr/^{86}Sr)_i$ ratio of 0.705697–0.706446 and $(^{143}Nd/^{144}Nd)_t$ ratio between 0.512562 and 0.512654. The mafic-intermediate rocks show more depleted Sr and enriched Nd isotopic compositions $(^{87}Sr/^{86}Sr)_i$ of 0.705123–0.705311 and $(^{143}Nd/^{144}Nd)_t$ ratio between 0.512653 and 0.512665. The enclaves have

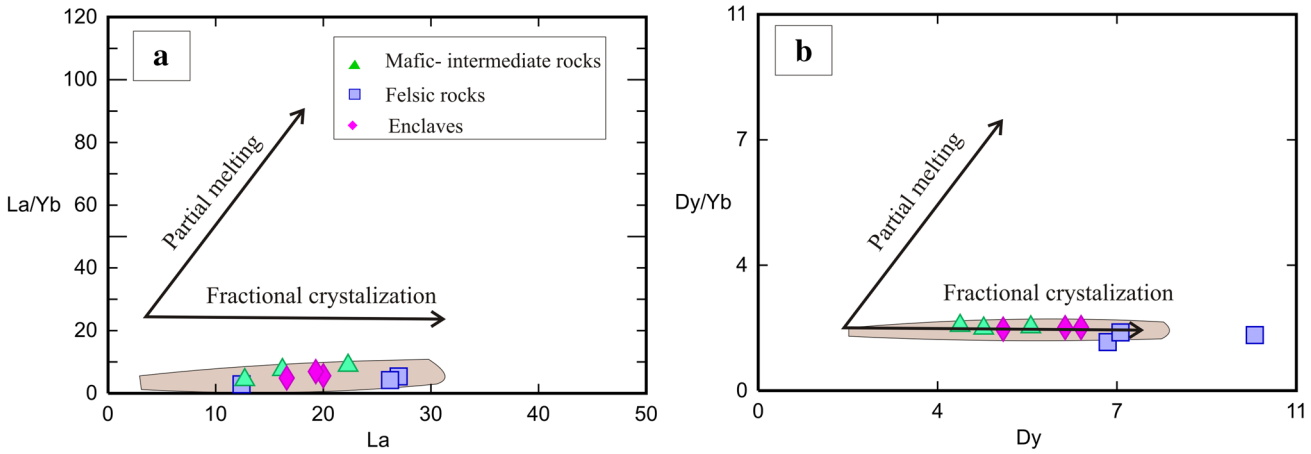

Fig. 7 **a** La/Yb vs. La. **b** Dy/Yb vs. Yb diagrams illustrating trends of partial melting vs. fractional crystallization processes (Gao et al. 2007). Shaded field represents compositions of the Zafarghand complex (Sadeghian and Ghaffary 2011)

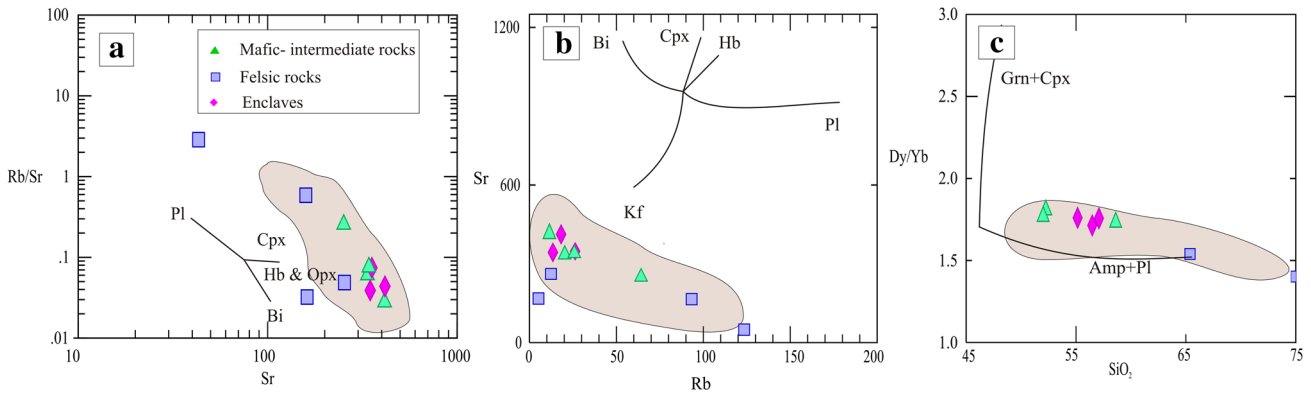

Fig. 8 **a** Rb/Sr vs. Sr (after Geng et al. 2009). **b** Sr vs. Rb (Osterhus et al. 2014). **c** SiO_2 vs. Dy/Yb diagrams (Davidson et al. 2007; Macpherson 2008) showing trends of fractional crystallization of plagioclase and amphibole for the samples from the Zafarghand complex. Shaded field represents compositions of the Zafarghand complex (Sadeghian and Ghaffary 2011)

Table 2 Sr and Nd isotopic data from the Zafarghand igneous complex

Samples	ZG1	ZG3	ZG4	ZD2	ZD3	ZE1	ZE2	ZE3
$^{87}Sr/^{86}Sr$	0.705864	0.705729	0.706716	0.705197	0.705930	0.705836	0.708545	0.705992
$^{143}Nd/^{144}Nd$	0.512642	0.512678	0.512583	0.512691	0.512677	0.512691	0.512670	0.512681
$^{87}Sr/^{86}Sr$ (i)	0.705787	0.705697	0.706446	0.705123	0.705311	0.705797	0.705533	0.705950
$^{143}Nd/^{144}Nd(T)$	0.512619	0.512654	0.512562	0.512665	0.512653	0.512668	0.512648	0.512657
$\varepsilon Nd_{(T)}$	0.08	0.75	−1.04	0.97	0.74	1.03	0.64	0.83
TDM1	1.01	1.11	1.06	1.3	1.1	1.03	0.91	1.08
fSm/Nd	−0.30	−0.24	−0.33	−0.19	−0.25	−0.26	−0.32	−0.25

$\varepsilon Nd_{(T)} = [(^{143}Nd/^{144}Nd)^{t}_{sample}/(^{143}Nd/^{144}Nd)^{t}_{CHUR}) - 1)] \times 10{,}000$; $TDM = 1/\lambda \times \ln\{1 + [((^{143}Nd/^{144}Nd)_{sample} - 0.51315)/((^{147}Sm/^{144}Nd)_{sample} - 0.21317)]\}$; and $f\text{Sm/Nd} = (^{147}Sm/^{144}Nd)^{0}_{Sample})/(^{147}Sm/^{144}Nd)^{0}_{CHUR})] - 1$

$(^{87}Sr/^{86}Sr)_i$ ratio of 0.705533–0.705950 and $(^{143}Nd/^{144}Nd)_t$ ratio between 0.512648 and 0.512668 and are slightly different from felsic rock values.

The corresponding Nd model age (TDM) for the felsic unit is in the range of 1.01–1.10 Ga. The Nd model ages of mafic-intermediate are relatively similar to those from felsic unit (TDM = 1.1 Ga). The Nd model ages of enclaves vary from 0.91 to 1.08 Ga and are slightly lower than values for other rocks. The Nd model ages for rocks are acceptable with a limited range of Sm/Nd fractionation, expressed as the fSm/

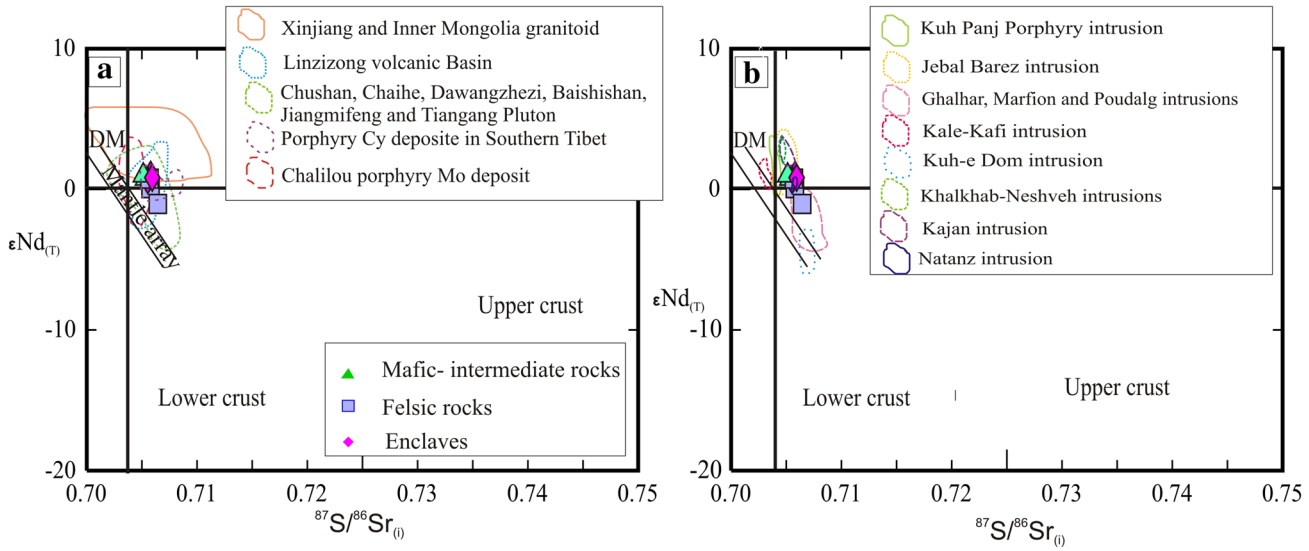

Fig. 9 $^{87}Sr/^{86}Sr_{(i)}$ vs. $^{143}Nd/^{144}Nd_{(t)}$ plots of isotopic ratios indicate the source for the magma from the Zafarghand complex and are compared with other igneous provinces

Nd value to the range of −0.2 to −0.6 (Wu et al. 2000), which is about −0.24 to −0.33 in the studied samples.

A comparison of Sr and Nd isotopic compositions of the ZIC with the orogenic belt of northern China to northeastern China, Xinjiang, Inner Mongolia granitoid (Wu et al. 1998); eastern part of the Central Asian Orogenic Belt, Chushan, Chaihe, Dawangzhezi, Baishishan, Jiangmifeng, and Tiangang plutons (Wu et al. 2000); the Paleogene Linzizong volcanic basin (Mo et al. 2008); porphyry Cu deposits in Southern Tibet (Chung et al. 2009; Hou et al. 2004); and Chalukou porphyry Mo deposit in northern Great Xing'an Range, NE China (Li et al. 2014) reveal isotopic similarities (Fig. 9a).

A comparison of isotopic composition of the ZIC with other igneous provinces in the UDMA from the Khalkhab–Neshveh intrusions (Rezaei-Kahkhaei et al. 2011); Ghalhar, Marfion, and Poudalg intrusions in Niyasar (Honarmand et al. 2014); Natanz intrusions (Haschke et al. 2010); Kajan intrusion (Golkaram et al. 2016); Kuh-e Dom intrusion (Kananian et al. 2014); Kal-e-Kafi intrusion (Ahmadian et al. 2016); and Kuh Panj and Jebal Barez intrusions in Kerman (Shafiei et al. 2009; Asadi et al. 2014) are also completed with descriptions of these intrusive rocks summarized in "Comparison with other cogenetic suites" (Fig. 9b).

Discussion

Petrogenesis of the mafic enclaves

Several hypotheses have been proposed to explain the origin of enclaves: (1) accidental country rock xenoliths (e.g., Maas et al. 1997; Bonin 2004); (2) the enclaves represent refractory (i.e. residual) phases after partial melting (e.g., White et al. 1999; Chappell et al. 2000); (3) autoliths, in which enclaves derived from cumulates of early-formed crystals and (or) chilled margins from a common parent (e.g., Dahlquist 2002; Donaire et al. 2005); or (4) products of magma mixing and mingling, with enclaves derived from a coeval mafic magma that intruded into the felsic magma chamber (Vernon 1984; Barbarin 2005; Yang et al. 2007; Li et al. 2014).

The enclaves are randomly distributed in the host granitoids and are oval, elongate, or irregularly shaped (Fig. 2a). These rocks display igneous microtextures, such as poikilitic–equigranular to microporphyritic without cumulate textures (Fig. 3). All these observations indicate that the mafic enclaves are not restites or xenoliths, because restites and xenoliths typically have metamorphic or residual fabrics (e.g., White et al. 1999). These enclaves cannot be attributed to cumulates either because of the absence of a cumulate texture (Barbarin 2005).

Donaire et al. (2005) believed that high ferromagnesian phase contents in MMEs show a cognate process, since nucleation rates of mafic phases are higher than quartz and feldspar, and thus, these phases become enriched as early crystallization products (Weinberg et al. 2001), whereas low mafic mineral contents and less than 50 vol.% in the studied enclaves are not supported by cognate genesis or chilled margins.

Fine-grained textures resulted from strong undercooling, high nucleation rates and, therefore, the relatively fine grain sizes typifying microgranular enclaves (Vernon 1990). In some cases, the MMEs have irregular chilled

margins against the host granitoids. However, the disintegration of larger enclaves, which had chilled margins, could generate many smaller ones that lack chilled margins (Dorais et al. 1990; Bonin 2004). Chilled margins in the enclaves also can imply significant contrasts in both temperature and viscosity between enclave and host melt that may be caused by rapid cooling of the mafic enclave components (e.g., Sarjoughian et al. 2012).

The elongate and irregular shapes of the microgranular enclaves in the host granitoids, which suggests that they deformed plastically within a partially crystallized convective magma (Yang et al. 2015a). The shape of the MMEs varies from rounded to ovoid, and having serrate or cuspate margins and partly diffuse contacts, with lobes convex towards the host rocks. The occurrence of both rounded and diffuse contacts in MMEs indicates that batches of magmas with a large variability in viscosity existed within the same magmatic system (Nittmann et al. 1985; Perugini et al. 2004). The hybrid zone (1–3 m) is also considered as felsic and mafic magmas forming network veining by their interaction, providing evidence for magma mixing events (Kim et al. 2002). In addition, the zones of lighter-coloured groundmass that are mantled by darker cores of some enclaves are consistent with some chemical exchange between enclaves and host (Pankhurst et al. 2011).

In addition, the presence of feldspar megacrysts in the enclaves is probably phenocryst captured from the partially crystalline host magma by the enclave magma (e.g., Vernon et al. 1988; Perugini et al. 2003) and is interpreted as evidence that they were in a liquid state, which allows the mechanical transfer of crystals from the host felsic magma into the mafic magma at some earlier stage of emplacement (e.g., Vernon et al. 1988; Waight et al. 2000; Perugini et al. 2003; Feng et al. 2014).

It seems that the presence of feldspar megacrysts in the enclaves indicates that there was only a small rheological difference between the two magmas, and this enabled the exchange of crystals between the felsic magma and the mafic magma (e.g., Barbarin and Didier 1992; Waight et al. 2000; Perugini et al. 2003; Yang et al. 2015a).

Pillow-like enclaves are suggestive of the enclaves forming as mafic magma blobs that formed during injection into the granitic host magma, then undergoing quenching against the cooler felsic host magma (Dorais et al. 1990; Bonin 2004; Cheng et al. 2012). In addition, schlieren structures strongly suggest interaction between two crystal-mush systems and rule out the possibility that the enclaves might have been totally solid at the time of interaction (Poli 1992). Some felsic veins occurring within the enclaves support the presence of a residual liquid and provide further evidence of magma mixing and mingling during enclave formation (e.g., Cheng et al. 2012).

Alternatively, several other lines of evidence indicate that these MMEs most likely represent globules of mafic magmas that were injected into magma chamber and mixed/mingled with cooler, partially crystallized host felsic magmas; (1) large plagioclase and K-feldspar crystals with corrosion embayments and cross-cutting the enclave/host boundary are considered as evidence that when the enclaves were in a liquid state when they were incorporated into the more felsic magma that would cause destabilization and consequently cause dissolution of these minerals; this accounts for the commonly rounded shapes of these phenocrysts in the host rocks (Vernon 1984, 1990; Vernon et al. 2004); (2) oscillatory or normally zoned plagioclase phenocrysts indicate variation in the crystallization conditions (e.g., Holten et al. 2000); (3) poikilitic texture in the K-feldspar megacrysts in the enclaves indicating that these crystals grew within melt, which during growth allows the incorporation of inclusion minerals by periodically attaching themselves to the faces of the growing crystals (e.g., Moore and Sisson 2008); (4) apatites in the enclaves display acicular features and are enclosed within the larger crystals, thus indicating that the mafic magma was rapidly quenched and cooled in the host granitic magma and can be a good proxy for magma mingling (e.g., Sparks and Marshall 1986; Piccoli and Candela 2002; Pankhurst et al. 2011); (5) mafic clots are a major sign of magma mixing and hybridization (e.g., Didier 1987; Vernon 1991); and (6) coexistence of two types of plagioclase possibly record the mixing of coexisting mafic and felsic magmas (e.g., Kaygusuz et al. 2008). Field and textural evidence indicate that the entrained enclaves and the granitic host were partially molten at the same time and suggested that magma mixing played a key role in the generation of these rocks resulting in the formation of fragments whose dimension varies from a few millimetres to metres in size.

Magma mixing/mingling and chemical exchange

Frost and Mahood (1987) has recommended two scenarios for the interaction of two contrasting magmas, such as: (1) the two magmas mix, thereby forming a hybrid melt and (2) the melts partially mix, but incompletely, whereas new mafic magma pulsed injections invaded the felsic magma chamber, forming MMEs. Mixing of two magmas is controlled by their bulk compositional and thermal differences (McBirney 1980; Furman and Spera 1985). Large compositional and thermal differences between the two magmas inhibit physical mingling, whereas smaller differences permit hybridization and chemical mixing. Rheologic modeling by Frost and Mahood (1987) indicates that homogenization of two magmas is unlikely if the compositional difference between them exceeds 10 wt% SiO_2. Of course, some researchers (e.g., Philpotts et al. 1998; Martin et al. 2006) recommended that the crystal content of a magma appears to be a critical

parameter controlling its mixing capacities, due to its effect on the viscosity of magmas (cf. Laumonier et al. 2014a).

It is possible that mafic magma mixed with felsic magma before extensive crystallization of the felsic magma. The nature and timing of chemical exchange have implications for emplacement and cooling histories and the relative temperature, composition, and degree of crystallization of the two magmas control their relative viscosities and the degree of physical mingling and chemical mixing of the two magmas (Sparks and Marshall 1986). Because the basic magma is hotter and less viscous than the acidic magma, the interacting basic and acid magmas would remain as distinct physical entities until they reach thermal equilibrium and (or) comparable viscosities (e.g., Campbell and Turner 1985). During the attainment of equilibrium, the basic magma simultaneously experiences rapid crystallization (quenching), during which it chemically evolves. Thermal exchange is more rapid than mechanical or chemical exchange, by about three to five orders of magnitude in silicate melts (Fernandez and Barbarin 1991; Barbarin and Didier 1992) and chemical exchange generally act after thermal equilibration. The diffusion of elements between the mafic and felsic magma tends towards a compositional equilibrium (Debon 1991).

In studying the interactions of enclaves and host magmas, two processes need to be considered: First infiltration and mixing of melt and phenocrysts occurred from the host with the enclave and secondly diffusion between the solid and liquid phases (Holden et al. 1991). Because when mafic magma injects into felsic magma and breaks up into globular enclaves, magma mingling and chemical diffusion would tend to modify the original composition of the enclave magma (Liu et al. 2015).

Of course, diffusive exchange of elements, such as K and Na, between a partial melt derived from xenoliths and the magma occurs at extremely rapid rates, can occur, with the magmas becoming contaminated by certain elements. In these systems, diffusion of Na out of the magma into the relatively Na-poor metasedimentary melt occurs and can change the ASI value of the magma as well, although Mg values remain constant (Erdmann and Clarke 2007). These features are not compatible with our geochemical results.

There is a clear correlation between the size of the enclaves and interaction degree between coeval magmas. The small-sized enclaves display fine-grained textures indicating rapid quenching, while the large enclaves reach up to 30 cm in diameter, display coarser grained textures, and higher felsic mineral contents in their rims. Chemical contrasts between small enclaves and the host granitoids are larger than between large enclaves and the host granitoids (Barbarin and Didier 1992). Due to rapid undercooling, small enclaves became a closed system relative to large enclaves (Yilmaz Sahin 2008). Therefore, the small mafic enclaves are less hybridized and have a more basic composition, whereas the large mafic enclaves were most likely hybridized by host granitic magmas.

A magma mingling and mixing origin for the enclaves is also testable using the geochemical data. Differences in major element compositions, combined with similarities in trace element and isotopic compositions, could reflect different diffusion rates of the elements during magma mixing (e.g., Dahlquist 2002; Yang et al. 2015a). Although it is difficult for major elements (except mobile elements such as K and Na) to diffuse and homogenize during magma mixing, major elements in the silicate melt are network-forming components and mainly in tetrahedral coordination, whereas trace elements and associated isotopic systems are non-network components that can be easily activated (Lesher 2010; Yang et al. 2015b).

In addition, Laumonier et al. (2014a) shows that diffusivity laws for the melt components at 1170 °C, self-diffusivities change from 10^{-12}–10^{-15} cm^2/s for Si; to 10^{-11}–10^{-14} cm^2/s for Al, Mg, and Ca; and up to 10^{-9} cm^2/s for Na and K, which correspond to diffusion distances per 1 h of 1–30 μm for Si; 10–200 μm for Al, Mg, and Ca; and 400–2000 μm for K and Na. However, the few experimental data available on multicomponent diffusion (e.g., Watson 1982), show that alkali diffusivities, in particular Na, decrease by up to three orders of magnitude (relative to self-diffusivity values), being comparable to those of Ca, Mg, or Al (i.e., 10^{-12}–10^{-13} m^2/s, Zhang et al. 2010).

Some researchers (e.g., Hofmann 1980; Baker 1989; Lesher 1994; Zhang et al. 2014a) believed that liquid-state isotope diffusion is up to two orders of magnitude more rapid than elemental diffusion and isotopic equilibration should approach a 1:1 correlation regardless of mineralogy (Holden et al. 1991). Lesher (1990) suggested that magma mixing via element diffusion would tend to modify fast diffusing Sr isotopes more effectively than Nd isotopes (e.g., Cheng et al. 2012) and the enclaves show a similar Sr isotopic composition relative to the host, indicating plagioclase was equilibrated with the melt (e.g., Ebertz et al. 1990; Flood and Shaw 2014). We conclude that the geochemical compositions of both mafic and felsic rocks have been affected by diffusive exchange processes, indicating a greater similarity of the Sr isotopic signature than of Nd isotopes. Subsequently, we suggest that the studied intrusion is a product of the partial chemical equilibration of felsic and mafic melts, representing a process of magma mixing/mingling.

A magma mixing/mingling model is also favoured by chemical discrimination techniques and analysis of mixing scenarios. The samples define hyperbolic mixing arrays (Yang et al. 2015a) in the MgO/Al_2O_3 vs. SiO_2/CaO diagram (Fig. 10a). The CaO/SiO_2 vs. FeO_t/SiO_2 (Fig. 10b; Berzina et al. 2014) and Ti/Zr vs. Sr/Zr diagrams (Fig. 10c; Karsli et al. 2007) also exhibit an array suggesting that mixed magma occured during ascent of these magmas.

The correlations between Ba/Ta and $^{87}Sr/^{86}Sr$ show decreasing trends (Fig. 10d; Hildreth and Moorbath 1988) and the correlations between $^{143}Nd/^{144}Nd$ and $^{147}Sm/^{144}Nd$ (Fig. 10e; Zhang et al. 2015) display an increasing trend can serve as evidence of magma mixing. Using the Th/Nb vs. Zr diagram (Fig. 10f), the studied samples define a vertical trend, indicating that magmatic evolution of these granitoids was controlled by bulk assimilation (BA) or magma mixing (Nicolae and Saccani 2003; El-Bialy and Omar 2015). These trends would be consistent with two-component mixing and is in accordance with field and petrographic evidence that there was some degree of physical and chemical interaction between the enclaves and the host granite, as discussed above.

Constraints on the sources

Three models have been proposed for the petrogenesis of calc-alkaline I-type granitoids: (1) fractional crystallization of mantle-derived magma with or without contamination (e.g., Petford and Atherton 1996); (2) partial melting of old basic-intermediate meta-igneous lower crust with or without interaction with mantle-derived mafic magmas (e.g., Rapp and Watson 1995); and (3) partial melting of the juvenile lower crust (e.g., Wu et al. 1998, 2000, 2006; Jahn et al. 2000, 2015; Li et al. 2014). Samples from the ZIC present a wide range of silica contents (SiO_2 = 52.01 to 77.56 wt%), as well as relatively low Mg# (ranging from 8 to 42). Sr–Nd isotopes [$^{87}Sr/^{86}Sr_{(i)}$ ranging from 0.705123 to 0.705950 and $\varepsilon Nd_{(T)}$ ranging from − 1.04 to + 1.03] compositions. Consequently, their parental magmas do not represent end-members of either primary mantle melts and (or) end-member lower continental crust.

In the La/Nb vs. Ba/Nb (Fig. 11a; Dilek et al. 2010), Th/Ta vs. La/Yb (Fig. 11b; Berzina et al. 2014), Th/U vs. Th (Fig. 11c; Kaygusuz et al. 2014), and Nb/Ta vs. Zr/Hf (Fig. 11d; Yang et al. 2008) diagrams, the compositions of the rocks from the studied complex plot between continental crust-derived melts and primitive mantle- and MORB-derived melts. In addition, $(La/Sm)_N$ in the studied complex are between crust [continental crust: 4.25; Weaver and Tarney (1984)] and mantle values [1.00; Sun and McDonough (1989)] and the average of $(La/Sm)_N$ ratios in the studied samples are 2.24, suggesting the role of both mantle and continental crust in the evolution of these magmas.

Typical amphibolites have positive εNd values that are quite similar to the εNd_i obtained for the studied intrusion (e.g., Moita et al. 2015). Likewise, some researchers (e.g., Wu et al. 1998, 2000, 2006; Jahn et al. 2000, 2015) believed that the geochemical characteristics, such as low initial $^{87}Sr/^{86}Sr$ ratios (0.705 ± 0.001), positive $\varepsilon Nd_{(T)}$ values (+ 4–0), and relatively young TDM model ages (912–1115 Ma) in the intrusive rocks indicate that originated from the juvenile crust. In addition, the moderately fractionated REE pattern of the granitoid suites, together with the undepleted and flat HREE patterns with $(Dy/Yb)_{CN}$ ratios of 1–1.18, is incompatible with partial melting of a garnet-bearing source (Guo et al. 2009) and

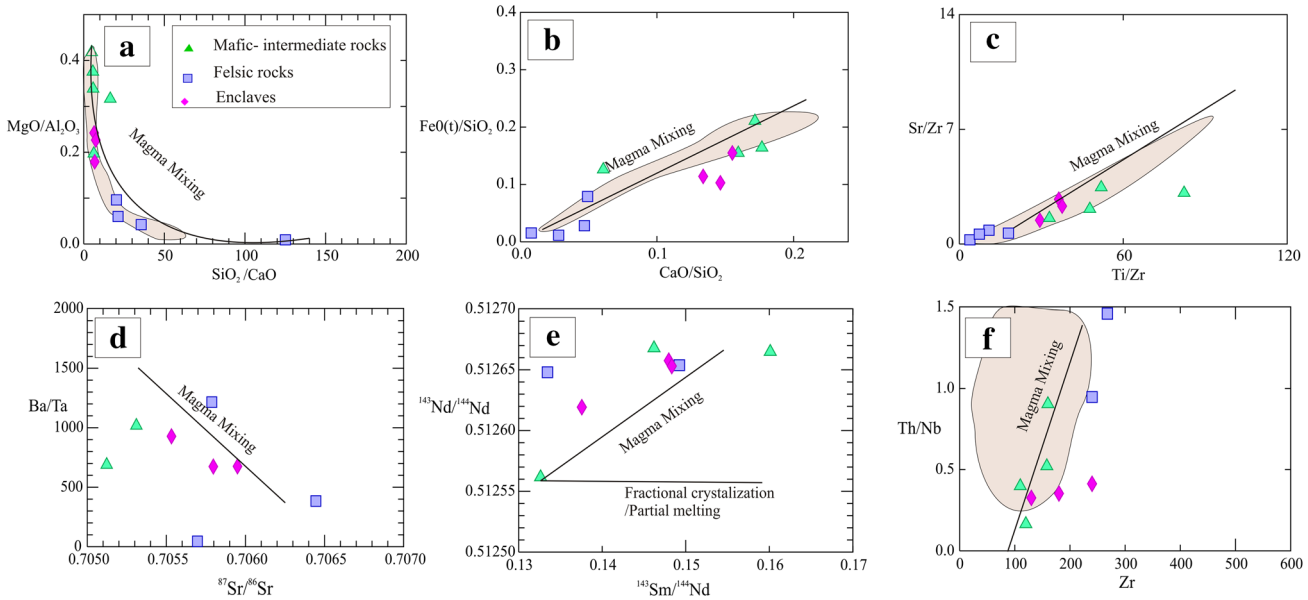

Fig. 10 **a** SiO_2 vs. MgO/Al_2O_3 (Yang et al. 2015a). **b** CaO/SiO_2 vs. $FeO_{(t)}/SiO_2$ (Berzina et al. 2014). **c** Ti/Zr vs. Sr/Zr (Karsli et al. 2007). **d** $^{87}Sr/^{86}Sr$ vs. Ba/Ta (Hildreth and Moorbath 1988). **e** $^{143}Sm/^{144}Nd$ vs. $^{143}Nd/^{144}Nd$ (Zhang et al. 2015). **f** Zr vs. Th/Nb (Nicolae and Saccani 2003) plots indicating the role of magma mixing/mingling in the Zafarghand complex. Shaded field represents compositions of the Zafarghand complex (Sadeghian and Ghaffary 2011)

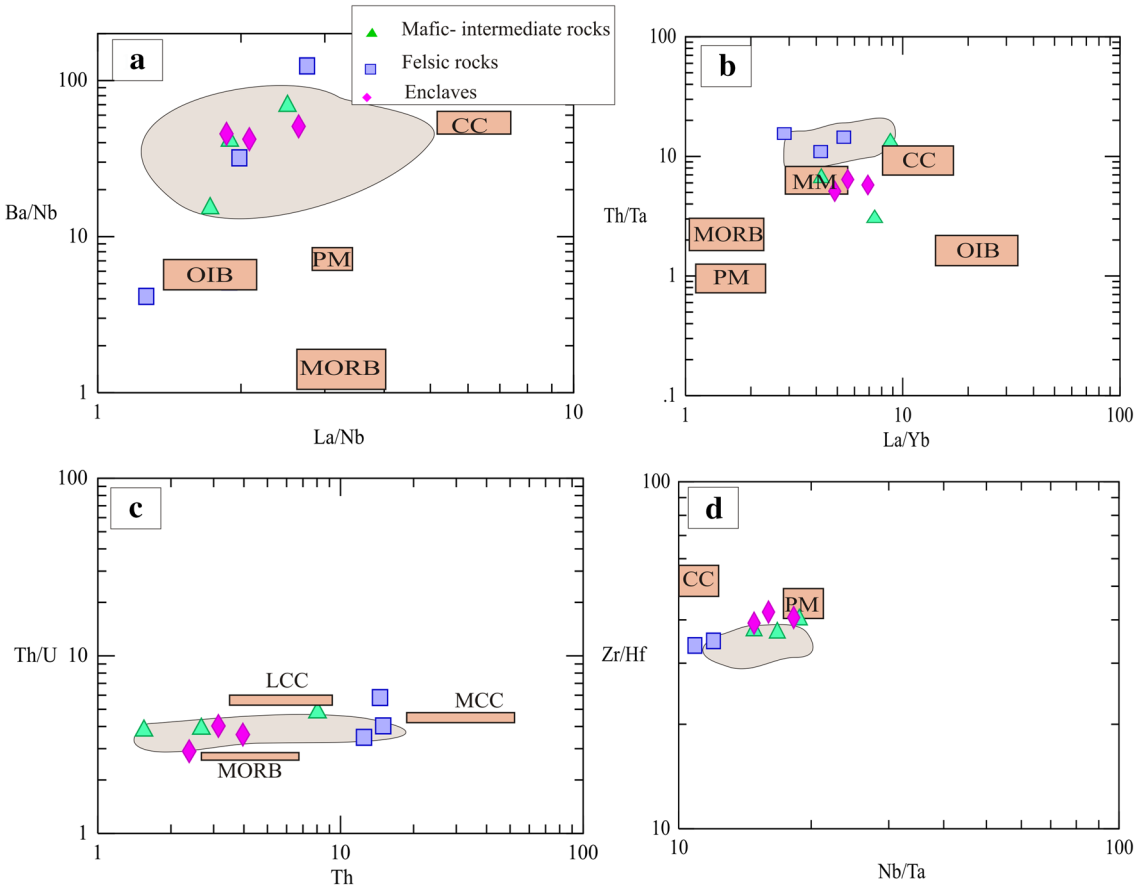

Fig. 11 Studied samples plotted on: **a** La/Nb vs. Ba/Nb. **b** La/Yb vs. Th/Ta, **c** Th vs. Th/U. **d** Nb/Ta vs. Zr/Hf diagrams used to distinguish between different source rocks. *PM* primitive mantle, *MORB* mid oceanic ridge basalt, *OIB* oceanic island basalt, *MM* metasomatized mantle [values are from Sun and McDonough (1989)], *CC* continental crust, *MCC* middle continental crust, *LCC* lower continental crust [values are from Rudnick and Gao (2003)]. Shaded field represents compositions of the Zafarghand complex (Sadeghian and Ghaffary 2011)

indicates that pyroxene and (or) amphibole are present in the source region at < 40 km depth (Liu et al. 2015). The results of these analyses demonstrate that the ZIC may have been generated by the partial melting of relatively juvenile crust with isotopic and geochemical signatures near those of the mantle.

To evaluate the source character of the parental magma of the ZIC, binary isotopic modeling has been employed with the use of upper mantle (UM) and medium/lower continental crustal (LCC/MCC) end-members and also basalt (B) and medium/lower continental crustal (LCC/MCC) end-member compositions. The isotopic modeling scheme is presented in Fig. 12, in which Sr and Nd isotopic bulk mixing lines plot between basalt (juvenile crust with metabasaltic and amphibolite composition) and old medium/lower continental crustal end-member. The proportions of the incorporated end-members, the modelling results, demonstrate that ~ 90–80% of the basaltic magma seems to have mixed with the lower/medium-crust-derived

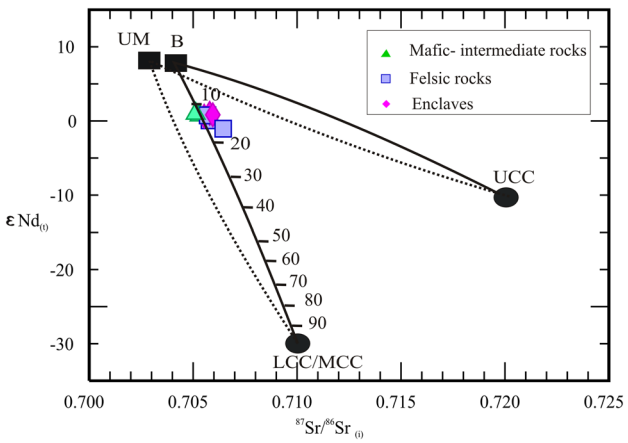

Fig. 12 Simple mixing model diagram showing a trend of $\varepsilon Nd_{(t)}$ vs. $(^{87}Sr/^{86}Sr)_i$ isotope variation of the Zafarghand complex. *UM* upper mantle, *LCC* lower continental crust, *MCC* middle continental crust, *UCC* upper continental crust, *B* basalt

magma (~ 10–20%) in the generation of the magmas with minimal upper crustal components added to the magma (Jahn et al. 1999).

The juvenile crustal source can be interpreted by three different methods: (1) partial melting of a subducted oceanic crust (e.g., Defant and Drummond 1990); (2) oceanic basaltic crustal materials atop the subducting/underthrusting oceanic lithosphere (Mo et al. 2008); and (3) mantle-derived juvenile continental crust (e.g., Wu et al. 1998, 2000).

The partial melting of subducted young oceanic crust is geochemically characterized by low Y and Yb and high Sr/Y (≥ 40) and La/Yb (≥ 20) ratios, which are indicative of garnet in their residual source and also has lower initial $^{87}Sr/^{86}Sr$, and higher $^{143}Nd/^{144}Nd$ than the studied samples, therefore, are not consistent with the ZIC.

On the other hand, Mo et al. (2008) believed that melting of oceanic basaltic crustal materials atop the subducting/underthrusting oceanic lithosphere could produce primary melts of andesitic compositions with inherited mantle isotopic signatures and melting of the more felsic materials including terrigenous sediments along with the subducting/underthrusting oceanic crust can produce more felsic melts. If amphibolitic slabs melt at these shallow levels, the melt would have no garnet signature and as a result offer no convincing geochemical evidence for slab melting, which has some key implications for the initial collisional setting; however, it may not seem likely because of the long distance to the trench (~ 100 km).

Another possibility is the development of juvenile crust during crustal growth had been previously stored (underplated) at the base of the crust, during compressional subduction (Taylor and McLennan 1985, 1995; Wu et al. 2000) and (or) initial collision.

All these observations support a genetic model, in which mantle-derived hydrous melt was emplaced as a succession of sills, in a laterally extensive region in the lower crust generating a deep crustal hot zone (e.g., Annen et al. 2006). Incubation times between the injection of the first sill and generation of melts are controlled by the initial geotherm, magma input rate, and the emplacement depth (Annen et al. 2006). The deep crustal hot zone where confining pressures are high and warm country rock decreases the cooling rates of magma chambers, therefore, enables the magma chambers to undergo recharge (Lee et al. 2014). The dehydration melting of mafic meta-igneous (e.g., amphibolitic and metabasaltic) juvenile crustal and old continental crustal rocks, of which melts ascended to shallower crustal levels, generating a variety of rock types ranging from gabbro to granite.

Annen et al. (2006) believed that chemically hybrid melts can be formed if the residual melts from basalt crystallization are mixed with partial melts of older crust, within deep crustal hot zones during extraction. The experimental studies indicate dissolved H_2O contents from almost zero to 10 wt% (e.g., Sisson and Layne 1993; Carmichael 2002) and can generate a wide diversity of melt compositions.

A thermal anomaly induced by underplated basic magma into the lower crust would have caused amphibolite and metabasaltic dehydration partial melting in the juvenile crust; partial melting of this juvenile crust generated these igneous rocks.

However, CaO, MgO, and Fe_2O_{3T} of the enclaves are generally higher, whereas the SiO_2 content and Nd model ages are lower than that of host rocks. It seems that the microgranular enclaves and mafic-intermediate rocks represent large volumes of basaltic-to-amphibolitic relatively juvenile crustal magmas, with the possibly of a minor mantle component, which once injected into the felsic magma, cools rapidly, partially crystallizes, and then becomes more viscous to form discrete magma blobs. The Sr–Nd isotopic ratios of the MMEs are similar to the host rocks, indicating that incomplete mixing of mafic and host granodioritic magmas caused local Sr–Nd isotopic equilibration, while major element disequilibrium is still evident (e.g., Allen 1991; Zhang et al. 2014b). With further injection of evolved mafic magmas into a melt-rich granitic mass, more complete magma mixing resulted in a homogeneously hybridized granodiorite. Later, injections into more fully crystallized hybrid rocks generated spheroidal MME, and hybridized magma evolved through fractional crystallization and possibly slight assimilation to form the acidic rocks.

Tectonic setting

Calc-alkaline rocks are the typical products of convergent plate margin tectonic settings. They are characterized by enrichment of LILE and Pb, distinct negative Nb, Ta, P, and Ti anomalies, LREE enrichment relative to MREE and HREE. These characteristics have commonly been explained by the addition of hydrous fluids released from subducting oceanic lithosphere, selectively enriched in LILE and other fluid-mobile elements (e.g., Pb and U), to the mantle wedge, lowering the mantle solidus and leading to magma generation, whereas HFS elements preferentially remain in stable accessory minerals (e.g., Saunders and Tarney 1984; Murphy 2007). In addition, the overall enrichments in LILEs and LREEs can also result from the interaction between mantle-derived melts with crust. Nevertheless, these geochemical characteristics, coupled with the Pb peak and Ti–Nb negative anomalies in the primitive mantle-normalized patterns and the Sr–Nd isotopic compositions, could be caused by magma mixing and (or) crustal contamination (Rollinson 1993).

Various tectono-magmatic discrimination diagrams are used to interpret the tectonic settings of the granitoids from the ZIC. Pearce et al. (1984) indicate that arc granites (I-type) have relatively low Rb and Y + Nb, as well

as low Yb + Ta contents; most of these samples plot in the field of volcanic arc granites (VAG) in Rb vs. Y + Nb and Yb + Ta diagrams, suggesting a subduction-related arc setting (Fig. 13a, b). Moreover, Thieblemont and Tegyey (1994) suggested that Nb/Zr ratio is reliable for distinguishing between different tectonic settings, especially subduction from collisional settings, with the low Nb/Zr ratio of these samples consistent with a subduction setting (Fig. 13c). The average Zr/Y ratio ranges from 5.86 in the felsic rocks, 5.36 in the intermediate-mafic rocks, and 5.23 in the enclaves are closely comparable to Zr/Y ratio calculated by Pearce and Norry (1979) for continental arcs (> 3).

It is clear that the geochemical properties of the ZIC are compatible with a convergent margin with the consumption of the Neotethyan Ocean, during formation of the UDMA, which was related to the development of the adjacent Sanandaj–Sirjan zone (Fig. 1). According to many researchers (e.g., Hooper et al. 1994; Hafkenscheid et al. 2006; Robertson et al. 2009; Chiu et al. 2013; Richards 2015), the timing of Arabia–Eurasia collision of the Arabian and Eurasian plates began in the Miocene at ~ 15–20 Ma (Agard et al. 2011); the subducting Neotethyan slab steepened due to to rollback of the slab and (or) there was slab break-off (see Agard et al. 2011); these geochemical signatures can also form in transpressional settings, generating the upwelling mantle resulting in selective partial melting (Fig. 14).

Comparison with other cogenetic suites

For more careful consideration and evaluating the possible source(s), the geochemical data of this study's samples were compared with other igneous provinces, such as some published data from the orogenic belt of northern China to northeastern China, Xinjiang, Inner Mongolia granitoids

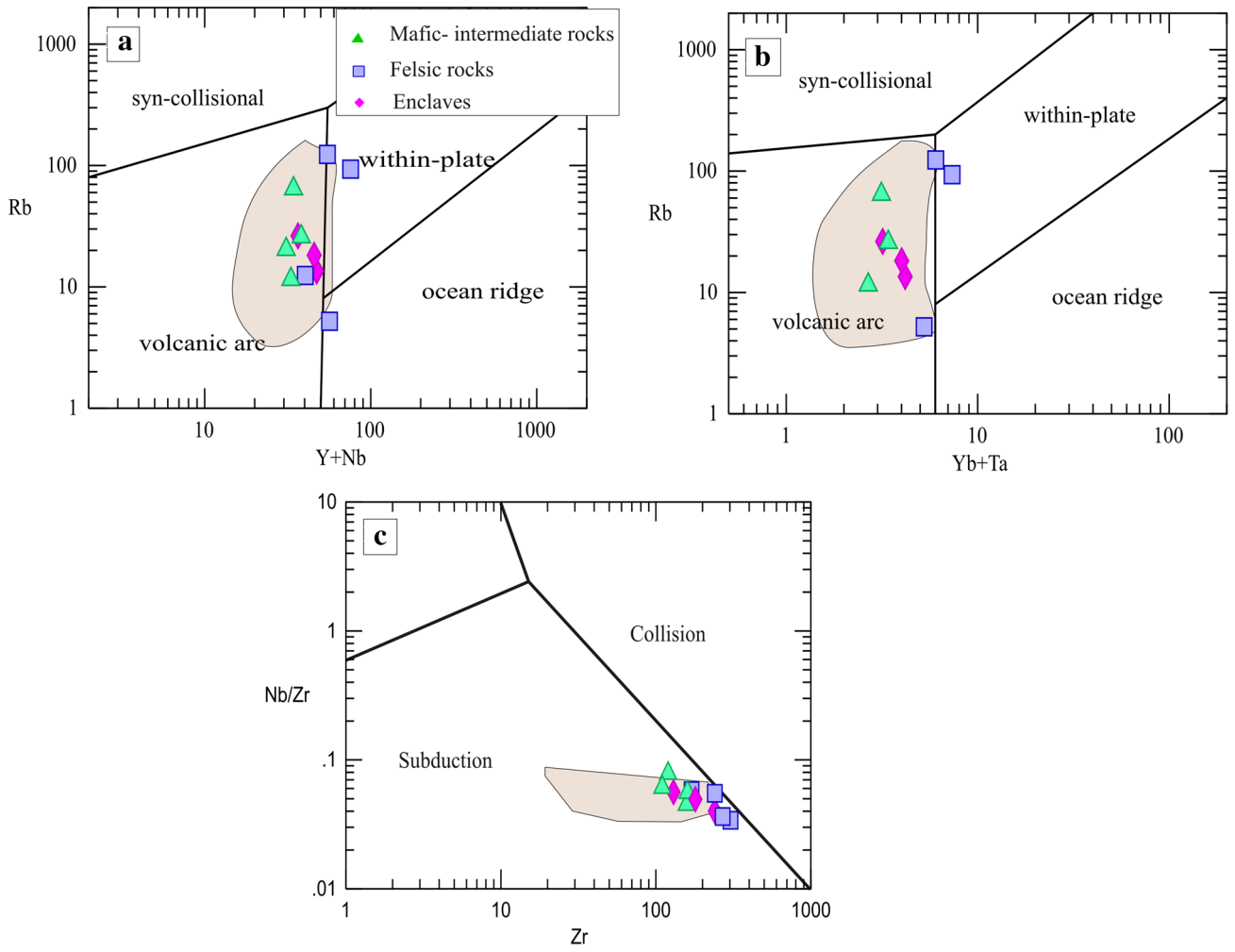

Fig. 13 **a, b** Distribution of the selected samples in the geotectonic discrimination diagrams of Pearce et al. (1984). **c** Thieblemont and Tegyey (1994). Christiansen and Keith (1996) noted that VAG, syn-COLG, and WPG are similar to I-type, S-type, and A-type granitoid varieties. Shaded field represents compositions of the Zafarghand complex (Sadeghian and Ghaffary 2011)

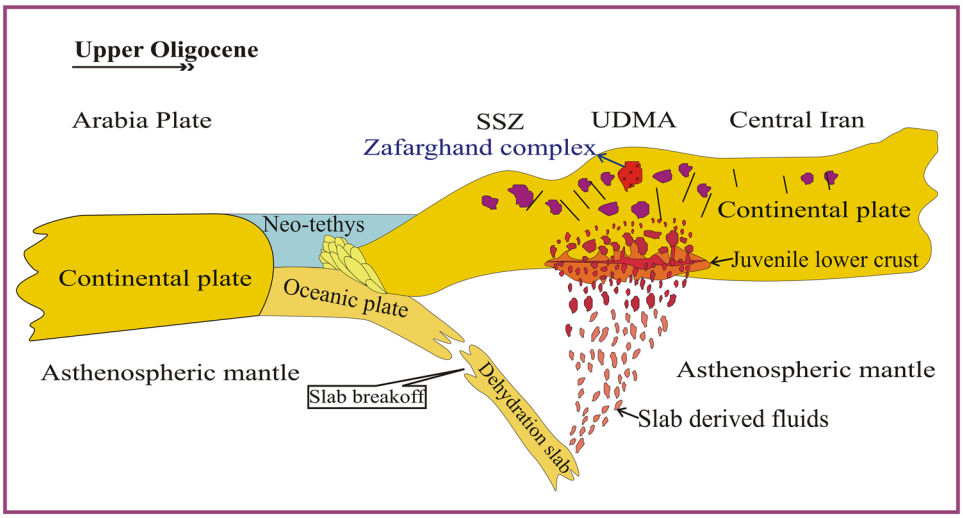

Fig. 14 Schematic illustration of the geodynamic evolution of the Central UDMA in the late Oligocene

(Wu et al. 1998); eastern part of the Central Asian Orogenic Belt, Chushan, Chaihe, Dawangzhezi, Baishishan, Jiangmifeng, and Tiangang plutons (Wu et al. 2000); the Paleogene Linzizong volcanic basin (Mo et al. 2008); porphyry Cu deposits in Southern Tibet (Hou et al. 2004; Chung et al. 2009); and Chalukou porphyry Mo deposit in northern Great Xing'an Range, NE China (Li et al. 2014) that have similar geochemical and isotopic signatures. The porphyry Cu deposits in southern Tibet (Hou et al. 2004; Chung et al. 2009) and Chalukou porphyry Mo deposit in northern Great Xing'an Range, NE China (Li et al. 2014), however, exhibit relatively high Sr/Y and La/Yb ratios similar to adakites rocks. As shown in Fig. 9a, the studied samples and Paleogene Linzizong volcanic basin (Mo et al. 2008), eastern part of the Central Asian Orogenic Belt (Wu et al. 2000), Chalukou porphyry Mo deposit in northern Great Xing'an Range, NE China (Li et al. 2014), and porphyry Cu deposits in southern Tibet (Hou et al. 2004; Chung et al. 2009) plot mostly in the right quadrants on a conventional Sr–Nd isotope diagram and overlap with each other (Fig. 9a); this indicates that the melts were derived from juvenile crust with relatively young model ages (see also Jahn et al. 2000; Wu et al. 2006). The isotope data preclude the possibility of melt derivation from ancient basement, revealing a large proportion of juvenile components in the magma source. As partial melting of juvenile lower crust, probably amphibolites and metabasaltic, along with minor mantle and (or) upper crust together with extensive crystal fractionation contributed to the formation of these intrusive rocks.

Comparison with other intrusions in the UDMA

As noted above, the upper Oligocene ZIC belongs to the UDMA, which formed from the subduction between Arabia and Eurasia, although in a locally extensional regime. The geochemical data of the studied samples were compared with other igneous provinces in the UDMA in the Central Iran, such as Khalkhab–Neshveh (Rezaei-Kahkhaei et al. 2011); Ghalhar, Marfion, and Poudalg (Honarmand et al. 2014); Natanz (Haschke et al. 2010); Kajan (Golkaram et al. 2016); Kuh-e Dom (Kananian et al. 2014); Kal-e-Kafi (Ahmadian et al. 2016); and Kuh Panj and Jebal Barez (Shafiei et al. 2009; Asadi et al. 2014) intrusions. Geochemical and isotopic data indicate that all igneous provinces are metaluminous, calc-alkaline, with an I-type arc geochemical affinity and are relatively similar to their other geochemical properties, such as trace and REE abundances.

The Late Eocene Khalkhab–Neshveh intrusion also consists of a wide spectrum from quartz monzogabbro to granite. Rezaei-Kahkhaei et al. (2011) proposed that this intrusion might have been derived from metasomatized mantle or lower continental crust.

The Ghalhar, Marfion, and Poudalg intrusions in Niyasar are comprised of early Eocene microdiorite, early Oligocene dioritic sills, and middle Miocene tonalite, quartz diorite, and diorite. Geochemical and isotopic evidence for these Eocene–Oligocene mafic rocks suggests that the magmas originated from lithospheric mantle with significant involvement of an EMII component and were strongly affected by crustal contamination, and the middle Miocene granitoids also suggest a mixed mantle–crustal origin (Honarmand et al. 2014).

The Natanz intrusion composed of Eocene granites and Miocene gabbro, diorite, granodiorite, and granite has geochemical characteristics indicating a change in the mineralogy of the residual melt, from the garnet-bearing amphibolite to metasomatized mantle peridotite (Haschke et al. 2010).

The Neogene Kajan igneous rocks are comprised of quartz diorite, quartz monzodiorite, tonalite, and granite. Golkaram et al. (2016) suggested an important contribution

from the mantle wedge source with minor interaction with the upper crust for the most evolved felsic rocks.

The Eocene Kuh-e Dom multiphase intrusion has a wide range of compositions from granite and granodiorite, to diorite and gabbro. This geochemical and isotopic evidence indicates a mixed origin for the Kuh-e Dom hybrid granitoid with a range of contributions of both the crust and mantle, most probably by the interaction between lower crust- and mantle-derived magmas (Kananian et al. 2014).

The Eocene Kal-e-Kafi intrusions range in composition from gabbro to granite. These granitoid rocks show some affinities with adakites, e.g., high Sr/Y and La/Yb ratios. Geochemical characteristics indicate that these rocks were probably derived by the partial melting of delaminated lower crust, which interacted with the surrounding metasomatized peridotite mantle with a composition of garnet-bearing amphibolite or amphibole-bearing eclogite melting (Ahmadian et al. 2016).

Tertiary intrusive activity in the Kerman was concentrated in two distinct episodes: (1) Eocene–Oligocene (Jebal Barez) composite gabbroic to granitic barren intrusions and (2) mid–late Miocene (Kuh Panj) dioritic to granodioritic stocks. The Kuh Panj intrusion exhibits relatively high Sr/Y and La/Yb ratios, similar to adakites rocks. Geochemical modeling indicates peridotite partial melting for the Eocene–Oligocene intrusions and a hydrous garnet-bearing amphibolite juvenile lower crust source for middle-late Miocene intrusions (Shafiei et al. 2009; Asadi et al. 2014).

The Kajan intrusion (Golkaram et al. 2016); Khalkhab–Neshveh intrusions (Rezaei-Kahkhaei et al. 2011), Miocene Natanz, (Haschke at al. 2010), and Jebal Barez and Kuh Panj intrusive rocks (Shafiei et al. 2009; Asadi et al. 2014) with young Nd model ages, mostly plot in the right quadrants, near the horizontal line on a conventional Sr–Nd isotope diagram and overlap with each other; however, the Kuh-e Dom (Kananian et al. 2014), Ghalhar, Marfion, and Poudalg (Honarmand et al. 2014) samples show differences in isotopic ratios and are characterized by higher initial $^{87}Sr/^{86}Sr$ and lower $^{143}Nd/^{144}Nd$ than the ZIC and the Kal-e-Kafi samples (Ahmadian et al. 2016) that also reveal lower initial $^{87}Sr/^{86}Sr$ than typical within ZIC. The Sr–Nd features of the studied samples are comparable to those of Kajan, Khalkhab–Neshveh, Miocene Natanz, Jebal Barez, and Kuh Panj intrusions (Fig. 9b), which indicates that the melts could be cogenetic.

This geochemical and isotopic evidence support a mixed origin for the lower middle Eocene Kuh-e Dom and middle Miocene Ghalhar, Marfion, and Poudalg intrusions with a range of contributions of both the old lower crust and mantle. They are generated by partial melting of variable portions of mafic lower crust and mantle, with some crustal contamination during magma ascent, although have different ages (Honarmand et al. 2014; Kananian et al. 2014). In addition, the Kal-e-Kafi intrusion shows some affinities with adakites generated near the boundary between garnet-bearing amphibolite or amphibole-bearing eclogite melting zone of the delaminated lower crust, at pressures equivalent to crustal thicknesses of > 40 km (Ahmadian et al. 2016). Whereas Kajan, Khalkhab–Neshveh, Miocene Natanz, Jebal Barez, and Kuh Panj intrusions could be a result of melting from the relatively juvenile mafic lower crust. If it is accepted that the Kajan, Khalkhab–Neshveh, Miocene Natanz, Jebal Barez, and Kuh Panj intrusions are mainly derived from partial melting of relatively juvenile mafic lower crust, this then suggests that new crustal growth is an important growth mechanism in the central UDMA.

Conclusions

The following conclusions can be drawn from the petrological and geochemical data discussed above:

1. The Upper Oligocene Zafarghand igneous complex (ZIC) is located in the UDMA and is comprised of gabbro to granite with abundant rounded enclaves with sharp, crenulated, and (or) diffuse contacts and feldspar megacrysts, which are interpreted as evidence for coexisting mafic and felsic magmas.
2. Disequilibrium textures, such as oscillatory-zoned plagioclases, resorbed plagioclase megacrysts, small lath-shaped plagioclase in large plagioclase, mafic clots, poikilitic texture in K-feldspar megacrysts, and acicular apatite, can be interpreted to reflect interaction of magmas to form diverse chemical compositions.
3. The differences in major-element composition and similarities in trace-element and isotopic compositions may reflect different diffusion rates of the elements during magma mixing. Likewise, the geochemical diagrams also support a mixing/mingling model between felsic and mafic magma.
4. Geochemical and isotopic data suggest that the mafic source involves melt interaction from dehydration melting of mafic amphibolitic and metabasaltic juvenile crustal (~ 80–90%) and old lower/middle crustal components (~ 10–20%), with pyroxene and (or) amphibole composition that are present in the source region without garnet.
5. Consequently, the ZIC in the UDMA represents a continental margin setting, which was emplaced during subduction of the Neotethys Ocean beneath the Sanandaj-Sirjan and Central Iran zones. However, rollback of the slab and (or) slab break-off possibly with transpression may have resulted in a locally extensional emplacement regime.

Acknowledgements Thanks go to the University of Kurdistan for supporting this project under grants provided by the research council (number: 4.64500; date: 3/11/2015). This study was also financially supported by the "National Natural Science Foundation of China (41472192)", and the State Key Laboratory of Lithosphere Evolution (11232240). DL is supported by a NSERC Discovery grant. This is a contribution to IGCP 592. We acknowledge Prof. Dr. Wolf-Christian Dullo, Prof. Greg Shellnutt, Prof. Saskia Erdmann, and anonymous reviewer for their constructive comments leading to important improvements in the manuscript.

References

Agard P, Omrani J, Jolivet L, Mouthereau F (2005) Convergence history across Zagros (Iran): constraints from collisional and earlier deformation. Int J Earth Sci 94:401–419

Agard P, Omrani J, Jolivet L, Whitechurch H, Vrielynck B, Spakman W, Monié P, Meyer B, Wortel R (2011) Zagros orogeny: a subduction-dominated process. Geol Mag 148:692–725

Ahmadian J, Sarjoughian F, Lentz D, Esna-Ashari A, Murata M, Ozawa H (2016) Eocene K-rich adakitic rocks in the Central Iran: implications for evaluating its Cu–Au–Mo metallogenic potential. Ore Geol Rev 72:323–342

Alavi M (1994) Tectonics of the Zagros orogenic belt of Iran; new data and interpretations. Tectonophysics 229:211–238

Alavi M, Mahdavi MA (1994) Stratigraphy and structure of the Nahavand region in western Iran and their implications for the Zagros tectonics. Geol Mag 131:43–47

Ali SA, Buckman S, Aswad KJ, Jones BG, Ismail SA, Nutman AP (2013) The tectonic evolution of a Neo-Tethyan (Eocene–Oligocene) island-arc (Walash and Naopurdan groups) in the Kurdistan region of the Northeast Iraqi Zagros Suture Zone. Isl Arc 22:104–125

Allen MB (1991) Local equilibrium of mafic enclaves and granitoids of the Turtle pluton, southeast California: mineral, chemical, and isotopic evidence. Am Miner 76:574–588

Allen MB (2009) Discussion on the Eocene bimodal Piranshahr massif of the Sanandaj-Sirjan zone, west Iran: a marker of the end of collision in the Zagros orogen. J Geol Soc Lond 166:981–982

Allen MB, Armstrong HA (2008) Arabia–Eurasia collision and the forcing of mid-Cenozoic global cooling. Palaeogeogr Palaeoclimatol Palaeoecol 265:52–58

Annen C, Blundy JD, Sparks RSJ (2006) The genesis of intermediate and silicic magmas in deep crustal hot zones. J Petrol 47:505–539

Ao S, Xiao W, Khalatbari Jafari M, Talebian M, Chen L, Wan B, Ji W, Zhang Z (2016) U–Pb zircon ages, field geology and geochemistry of the Kermanshah ophiolite (Iran): from continental rifting at 79 Ma to oceanic core complex at ca. 36 Ma in the southern Neo-Tethys. Gondwana Res 31:305–318

Asadi S, Moore F, Zarasvandi A (2014) Discriminating productive and barren porphyry copper deposits in the southeastern part of the central Iranian volcano-plutonic belt, Kerman region, Iran: a review. Earth Sci Rev 138:25–46

Bacon CR (1986) Magmatic inclusions in silicic and intermediate rocks. J Geophys Res 81:6091–6112

Baker DR (1989) Tracer versus trace element diffusion: diffusional decoupling of Sr concentration from Sr isotope composition. Geochim Cosmochim Ac 53:3015–3023

Ballato P, Uba CE, Landgraf A, Strecker MR, Sudo M, Stockli DF, Friedrich A, Tabatabaei SH (2011) Arabia–Eurasia continental collision: insights from late tertiary foreland-basin evolution in the Alborz Mountains, northern Iran. Geol Soc Am Bull 123:106–131

Barbarin B (2005) Mafic magmatic enclaves and mafic rocks associated with some granitoids of the central Sierra Nevada batholith, California: nature, origin, and relations with the hosts. Lithos 88:155–177

Barbarin B, Didier J (1992) Genesis and evolution of mafic microgranular enclaves through various types of interaction between coexisting felsic and mafic magmas. T Roy Soc Edin Earth 83:145–153

Berberian F, Berberian M (1981) Tectono-plutonic episodes in Iran. In: Gupta HK, Delany FM (eds) Zagros-Hindu Kush-Himalaya geodynamic evolution, vol 3. Am Geophys Union Geodynamics Series, Washington, DC, pp 5–32

Berberian M, King GCP (1981) Towards a paleogeography and tectonic evolution of Iran. Can J Earth Sci 18:210–265

Berzina AP, Berzina AN, Gimon VO (2014) Geochemical and Sr–Pb–Nd isotopic characteristics of the Shakhtama porphyry Mo–Cu system (Eastern Transbaikalia, Russia). J Asian Earth Sci 79:655–665

Beydoun ZR, Hughes Clarke MW, Stoneley R (1992) Petroleum in the Zagros Basin; a Late Tertiary foreland basin overprinted onto the outer edge of a vast hydrocarbon-rich Paleozoic-Mesozoic passive-margin shelf. AAPG Mem 55:309–339

Blundy JD, Sparks RSJ (1992) Petrogenesis of mafic inclusions in granitoids of the Adamelo Massif, Italy. J Petrol 33:1039–1104

Bonin B (2004) Do coeval mafic and felsic magmas in post-collisional to within-plate regimes necessarily imply two constrasting, mantle and crust, sources? a review. Lithos 78:1–24

Campbell IH, Turner JS (1985) Turbolent mixing between fluids with different viscosities. Nature 313:39–42

Campbell IH, Turner JS (1986) The influence of viscosity on fountains in magma chambers. J Petrol 27:1–30

Carmichael ISE (2002) The andesite aqueduct: perspectives on the evolution of intermediate magmatism in west–central (105–99°W) Mexico. Contrib Miner Petrol 143:641–663

Chappell BW (1999) Aluminium saturation in I- and S-type granites and the characterization of fractionated haplogranites. Lithos 46:535–551

Chappell BW (2004) Towards a unified model of granite genesis. T Royal Soc Edin Earth 95:1–10

Chappell BW, White AJR (1991) Restite enclaves and the restite model. In: Didier J, Barbarin B (eds) Developments in petrology. Elsevier, Amsterdam, pp 375–381

Chappell BW, White AJR, Williams IS, Wyborn D, Wyborn LAI (2000) Lachlan Fold Belt granites revisited: high- and low-temperature granites and their implications. Aust Earth Sci 47:123–138

Chen B, Jahn BM, Wei C (2002) Petrogenesis of Mesozoic granitoids in the Dabie UHP complex, Central China: trace element and Nd–Sr isotope evidence. Lithos 60:67–88

Cheng Y, Spandler C, Mao J, Rusk BG (2012) Granite, gabbro and mafic microgranular enclaves in the Gejiu area, Yunnan Province, China: a case of two-stage mixing of crust- and mantle-derived magmas. Contrib Miner Petrol 164:659–676

Chiu HY, Chung SL, Zarrinkoub MH, Mohammadi SS (2013) Zircon U–Pb age constraints from Iran on the magmatic evolution related to Neotethyan subduction and Zagros orogeny. Lithos 162–163:70–87

Christiansen EH, Keith JD (1996) Trace-element systematics in silicic magmas: a metallogenic perspective. In: Wyman DA (ed) Trace element geochemistry of volcanic rocks: applications for massive sulfide exploration, vol 12. Geological Association of Canada, Short Course Notes, pp 115–151

Chung SL, Chu MF, Ji J, O'Reilly SY, Pearson NJ, Liu D, Lee TY, Lo CH (2009) The nature and timing of crustal thickening in southern Tibet: geochemical and zircon Hf isotopic constraints from postcollisional adakites. Tectonophysics 477:36–48

Clarke DB (1992) Granitoid rocks. Chapman and Hall, London
Çolakoğlu AR, Arehart GB (2010) The petrogenesis of Sarıçimen (Çaldıran-Van) quartz monzodiorite: implication for initiation of magmatism (Late Medial Miocene) in the east Anatolian collision zone. Turk Lithos 119:607–620
Dahlquist JA (2002) Mafic microgranular enclaves: early segregation from metaluminous magma (Sierra de Chepes), Pampean Ranges, NW Argentina. J S Am Earth Sci 15:643–655
Davidson J, Turner S, Handley H, Macpherson C, Dosseto A (2007) Amphibole "sponge" in arc crust? Geology 35:787–790
De la Roche H, Leterrier J, Grandclaude P, Marchal M (1980) A classification of volcanic and plutonic rocks using R1R2 diagram and major-element analyses—its relationships with current nomenclature. Chem Geol 29:183–210
Debon F (1991) Comparative major element chemistry in various "microgranular enclave–plutonic host" pairs. In: Didier J, Barbarin B (eds) Enclaves and granite petrology. Elsevier, Amsterdam, pp 293–312
Defant MJ, Drummond MS (1990) Derivation of some modern arc magmas by melting of young subducted lithosphere. Nature 347:662–665
Didier J (1987) Granites and their enclaves. Elsevier, Amsterdam
Dilek Y, Imamverdiyev N, Altunkaynak S (2010) Geochemistry and tectonics of Cenozoic volcanism in the Lesser Caucasus (Azerbaijan) and the peri-Arabian region: collision-induced mantle dynamics and its magmatic fingerprint. Inter Geol Rev 52:536–578
Domenick MA, Kistler RE, Dodge FCW, Tatsumoto M (1983) Nd and Sr isotopic study of crustal and mantle inclusions from the Sierra Nevada and implications for batholith petrogenesis. Geol Soc Am Bull 94:713–719
Donaire T, Pascual E, Pin C, Duthou JL (2005) Microgranular enclaves as evidence of rapid cooling in granitoid rocks: the case of the Los Pedroches granodiorite, Iberian Massif, Spain. Contrib Miner Petrol 149:247–265
Dorais MJ, Whitney JA, Roden MF (1990) Origin of mafic enclaves in the Dinkey Creek Pluton, Central Sierra Neveda Batholith, California. J Petrol 31:853–881
Drake MJ, Weill DF (1975) Partition of Sr, Ba, Ca, Y, Eu^{2+}, Eu^{3+} and other REE between plagioclase feldspar and magmatic liquid: an experimental study. Geochim Cosmochim Acta 39:689–712
Ebertz GW, Nicholls IA, Maas R, McCulloch MT, Whitford DJ (1990) The Nd and Sr isotopic composition of I-type microgranitoid enclaves and their host rocks from the Swifts Creek pluton, southeast Australia. Chem Geol 85:119–134
Eichelberger JC (1975) Origin of andesite and dacite: evidence of mixing at Glass Mountain in California and other circum Pacific volcanoes. Geol Soc Am Bull 86:1381–1391
El-Bialy MZ, Omar MM (2015) Spatial association of Neoproterozoic continental arc I-type and post-collision A-type granitoids in the Arabian–Nubian Shield: the Wadi Al-Baroud older and younger granites, north eastern desert, Egypt. J Afr Earth Sci 103:1–29
Erdmann S, Clarke DB (2007) The contamination of granitic magma by metasedimentary country-rock material: an experimental study. Can Miner 45:43–61
Feng SJ, Zhao KD, Ling HF, Chen PR, Chen WF, Sun T, Jiang SY, Pu W (2014) Geochronology, elemental and Nd–Hf isotopic geochemistry of Devonian A-type granites in central Jiangxi, South China: constraints on petrogenesis and post-collisional extension of the Wuyi–Yunkai orogeny. Lithos 206–207:1–18
Fernandez A, Barbarin B (1991) Relative rheology of coeval mafic and felsic magmas: nature of resulting interaction processes and shape and mineral fabrics of mafic microgranular enclaves. In: Didier J, Barbarin B (eds) Enclaves and granite petrology. Elsevier, Amsterdam, pp 63–275
Fershtater GB, Borodina NS (1977) Petrology of autoliths in granitic rocks. Inter Geol Rev 19:458–468
Flood RH, Shaw SE (2014) Microgranitoid enclaves in the felsic Looanga monzogranite, New England Batholith, Australia: pressure quench cumulates. Lithos 198–199:92–102
Frost TP, Mahood GA (1987) Field, chemical and physical constraints on mafic-felsic magma interaction in the Lamark granodiorite, Sierra Nevada, California. Geol Soc Am Bull 99:272–291
Frost BR, Barnes CG, Collins WJ, Arculus RJ, Ellis DJ, Frost CD (2001) A geochemical classification for granitic rocks. J Petrol 41:2033–2048
Furman T, Spera FJ (1985) Co-mingling of acid and basic magma with implications for the origin of I-type xenoliths: field and petrochemical relations of an unusual dike complex at Eagle Lake, Sequoia National Park. J Volcanol Geoth Res 24:151–178
Gao Y, Hou Z, Kamber BS, Wei R, Meng X, Zhao R (2007) Adakite-like porphyries from the southern Tibetan continental collision zones: evidence for slab melt metasomatism. Contrib Miner Petrol 153:105–120
Geng HY, Sun M, Yuan C, Xiao WJ, Xian WS, Zhao GC, Zhang LF, Wong K, Wu FY (2009) Geochemical, Sr–Nd and zircon U–Pb–Hf isotopic studies of Late Carboniferous magmatism in the West Junggar, Xinjiang: implications for ridge subduction? Chem Geol 266:373–398
Geshi N (2000) Fractionation and magma mixing within intruding dike swarm: evidence from the Miocene Shitara-Otoge igneous complex, central Japan. J Volcanol Geoth Res 98:127–152
Golkaram S, Rashidnejad–Omran N, Azizi H, Asahara Y, Buchsd DM, McDonald I, Santose FJ (2016) Petrogenesis and geodynamic evolution of the Kajan Neogene subvolcanic rocks, Nain, Central Iran. Chem Erde 76:567–578
Green TH, Pearson NJ (1985) Experimental determination of REE partition coefficients between amphibole and basaltic to andesitic liquids at high pressure. Geochim Cosmochim Acta 49:1465–1468
Guo F, Fan W, Li Ch, Gao X, Miao L (2009) Early Cretaceous highly positive εNd felsic volcanic rocks from the Hinggan Mountains, NE China: origin and implications for Phanerozoic crustal growth. Int J Earth Sci 98:1395–1411
Hafkenscheid E, Wortel MJR, Spakman W (2006) Subduction history of the Tethyan region derived from seismic tomography and tectonic reconstructions. J Geophys Res 111:B08401
Hanson GN (1980) Rare earth elements in petrogenetic studies of igneous systems. Annu Rev Earth Planet Sci 8:371–406
Haschke M, Ahmadian J, Murata M, McDonald I (2010) Copper mineralization prevented by arc-root delamination during Alpine–Himalayan collision in Central Iran. Econ Geol 105:855–865
Hassanzadeh J, Wernicke BP (2016) The Neotethyan Sanandaj-Sirjan zone of Iran as an archetype for passive margin-arc transitions. Tectonics 35:586–621
Hatzfeld D, Molnar P (2010) Comparisons of the kinematics and deep structures of the Zagros and Himalaya and of the Iranian and Tibetan plateaus and geodynamic implications. Rev Geophys 48:1–48
Hempton MR (1987) Constraints on Arabian Plate motion and extensional history of the Red Sea. Tectonics 6:687–705
Hildreth W, Moorbath S (1988) Crustal contributions to arc magmatism in the Andes of Central Chile. Contrib Miner Petrol 98:455–489
Hofmann A (1980) Diffusion in silicate melts. In: Hargraves RB (ed) Physics of magmatic processes. Princeton University Press, New York, pp 385–417
Holden P, Halliday AN, Stephens WE, Henney PJ (1991) Chemical and isotopic evidence for major mass transfer between mafic enclaves and felsic magma. Chem Geol 92:135–152
Holten T, Jamtveit B, Meakin P (2000) Noise and oscillatory zoning of minerals. Geochim Cosmochim Acta 64:893–1904

Honarmand M, Rashidnejad Omran N, Neubauer F, Emami MH, Nabatiand G, Liu X, Dong Y, Quadt A, Cheng B (2014) Laser-ICP-MS U–Pb zircon ages and geochemical and Sr–Nd–Pb isotopic compositions of the Niyasar plutonic complex, Iran: constraints on petrogenesis and tectonic evolution. Inter Geol Rev 56:104–132

Hooper RJ, Baron I, Hatcher RD, Agah S (1994) The development of the southern Tethyanmargin in Iran after the break-up of Gondwana-implications for the Zagros hydrocarbon province. Geoscience 4:72–85

Hou ZQ, Guo YF, Qu XM, Rui ZY, Mo XX (2004) Origin of adakitic intrusives generated during mid-Miocene east–west extension in southern Tibet. Earth Planet Sci Lett 220:139–155

Jahn BM, Wu F, Lo DH, Tsai CH (1999) Crust–mantle interaction induced by deep subduction of the continental crust: geochemical and Sr–Nd isotopic evidence from post-collisional mafic–ultramafic intrusions of the northern Dabie complex, central China. Chem Geol 157:119–146

Jahn BM, Wu F, Chen B (2000) Massive granitoid generation in Central Asia: Nd isotope evidence and implication for continental growth in the Phanerozoic. Episodes 23:82–92

Jahn BM, Valui G, Kruk N, Gonevchuk V, Usuki M, Wu JTJ (2015) Emplacement ages, geochemical and Sr–Nd–Hf isotopic characterization of Mesozoic to early Cenozoic granitoids of the Sikhote-Alin orogenic belt, Russian far east: crustal growth and regional tectonic evolution. J Asian Earth Sci 111:872–918

Kananian A, Sarjoughian F, Nadimi AR, Ahmadian J, Ling W (2014) Geochemical characteristics of the Kuh-e Dom intrusion, Urumieh–Dokhtar Magmatic Arc (Iran): implications for source regions and magmatic evolution. J Asian Earth Sci 90:137–148

Karagaranbafghi F, Foeken JPT, Guest B, Stuart FM (2012) Cooling history of the Chapedony metamorphic core complex, Central Iran: implications for the Eurasia–Arabia collision. Tectonophysics 524–525:100–107

Karsli O, Chen B, Aydin F, Sen C (2007) Geochemical and Sr–Nd–Pb isotopic compositions of the Eocene Dolek and Saricicek plutons, Eastern Turkey: implications for magma interaction in the genesis of high-K calc-alkaline granitoids in a post-collision extensional setting. Lithos 98:67–96

Kaygusuz A, Siebel W, Sen C, Satir M (2008) Petrochemistry and petrology of I-type granitoids in an arc setting: the composite Torul pluton, Eastern Pontides, NE Turkey. Inter Geol Earth Sci 97:739–764

Kaygusuz A, Arslan M, Siebel W, Sipahi F, İlbeyli N, Temizel İ (2014) LA-ICP MS zircon dating, whole-rock and Sr–Nd–Pb–O isotope geochemistry of the Camiboğazı pluton, Eastern Pontides, NE Turkey: implications for lithospheric mantle and lower crustal sources in arc-related I-type magmatism. Lithos 192–195:271–290

Keay S, Collins WJ, McCulloch MT (1997) A three-component Sr-Nd isotopic mixing model for granitoid genesis, Lachlan fold belt, eastern Australia. Geology 25:307–310

Kim JS, Shin KC, Lee JD (2002) Petrographical study on the Yucheon granite and its enclaves. Geosci J 6:289–302

Laumonier M, Scaillet B, Arbaret L, Champallier R (2014a) Experimental simulation of magma mixing at high pressure. Lithos 196:281–300

Laumonier M, Scaillet B, Pichavant M, Champallier R, Andujar J, Arbaret L (2014b) On the conditions of magma mixing and its bearing on andesite production in the crust. Nat Commun 5:5607

Lee CTA, Lee TC, Wu CT (2014) Modeling the compositional evolution of recharging, evacuating, and fractionating (REFC) magma chambers: Implications for differentiation of arc magmas. Geochim Cosmochim Acta 143:8–22

Lesher CE (1990) Decoupling of chemical and isotopic exchange during magma mixing. Nature 344:235–237

Lesher CE (1994) Kinetics of Sr and Nd exchange in silicate liquids: theory, experiments, and applications to uphill diffusion, isotopic equilibration, and irreversible mixing of magmas. J Geophys Res 99:9585–9604

Lesher CE (2010) Self-diffusion in silicate melts: theory, observations and applications to magmatic systems. Rev Miner Geochem 72:269–309

Li C, Li X, Li Q, Guo J, Li X, Yang Y (2012a) Rapid and precise determination of Sr and Nd isotopic ratios in geological samples from the same filament loading by thermal ionization mass spectrometry employing a single-step separation scheme. Anal Chim Acta 727:54–60

Li C, Li X, Li Q, Guo J, Li X, Feng L, Chu Z (2012b) Simultaneous determination of $^{143}Nd/^{144}Nd$ and $^{147}Sm/^{144}Nd$ ratios and Sm-Nd contents from the same filament loaded with purified Sm-Nd aliquot from geological samples by isotope dilution thermal ionization mass spectrometry. Anal Chem 84:6040–6047

Li ZZ, Qin KZ, Li GM, Ishihara S, Jin LY, Song GX, Meng ZJ (2014) Formation of the giant Chalukou porphyry Mo deposit in northern Great Xing'an Range, NE China: Partial melting of the juvenile lower crust in intra-plate extensional environment. Lithos 202–203:138–156

Liu Z, Jiang YH, Jia RY, Zhao P, Zhou Q (2015) Origin of Late Triassic high-K calc-alkaline granitoids and their potassic microgranular enclaves from the western Tibet Plateau, northwest China: implications for Paleo-Tethys evolution. Gondwana Res 27:326–341

Maas R, Nicholls IA, Legg C (1997) Igneous and metamorphic enclaves in the S-type Deddick granodiorite, Lachlan Fold Belt, SE Australia: petrographic, geochemical and Nd-Sr isotopic evidence for crustal melting and magma mixing. J Petrol 38:815–841

Macpherson CG (2008) Lithosphere erosion and crustal growth in subduction zones: insights from initiation of the nascent East Philippine Arc. Geology 36:311–314

Macpherson CG, Dreher ST, Thirlwall MF (2006) Adakites without slab melting: high pressure differentiation of island arc magma, Mindanao, the Philippines. Earth Planet Sci Lett 243:581–593

Maniar PD, Piccoli PM (1989) Tectonic discrimination of granitoids. Geol Soc Am Bull 101:635–643

Martin VM, Holness MB, Pyle DM (2006) The role of crystal frameworks in the preservation of enclaves during magma mixing. Earth Planet Sci Lett 248:787–799

McBirney AR (1980) Mixing and unmixing of magmas. J Volcanol Geoth Res 7:357–371

McKenzie D, O'Nions RK (1991) Partial melt distributions from inversion of rare earth element concentrations. J Petrol 32:1021–1091

McQuarrie N, van Hinsbergen D (2013) Retrodeforming the Arabia-Eurasia collision zone: age of collision versus magnitude of continental subduction. Geology 41:315–318

McQuarrie N, Stock JM, Verdel C, Wernicke BP (2003) Cenozoic evolution of Neotethys and implications for the causes of plate motions. Geophysl Res Lett 30:1–4

Mo X, Niu Y, Dong G, Zhao Z, Hou Z, Zhou S, Ke S (2008) Contribution of syncollisional felsic magmatism to continental crust growth: a case study of the Paleogene Linzizong volcanic Succession in southern Tibet. Chem Geol 250:49–67

Mohajjel M, Fergusson CL (2014) Jurassic to Cenozoic tectonics of the zagros orogen in northwestern Iran. Int Geol Rev 56:263–287

Mohajjel M, Fergusson CL, Sahandi MR (2003) Cretaceous–Tertiary convergence and continental collision Sanandaj–Sirjan zone Western Iran. J Asian Earth Sci 21:397–412

Moita P, Santos JF, Pereira MF, Costa M, Corfu F (2015) The quartz-dioritic Hospitais intrusion (SW Iberian Massif) and its mafic microgranular enclaves—evidence for mineral clustering. Lithos 224–225:78–100

Moore JG, Sisson TW (2008) Igneous phenocrystic origin of K-feldspar megacrysts in granitic rocks from the Sierra Nevada batholith. Geosphere 4:387–400

Murphy JB (2007) Igneous rock associations 8. Arc magmatism II: geo-chemical and isotopic characteristics. J Geol assoc Can 34:7–36

Nicolae I, Saccani E (2003) Petrology and geochemistry of the Late Jurassic calcalkaline series associated to Middle Jurassic ophiolites in the South Apuseni Mountains (Romania). Schweiz Miner Petrog Mitt 83:81–96

Nittmann J, Daccord G, Stanley HE (1985) Fractal growth of viscous fingers: quantitative characterization of a fluid instability phenomenon. Nature 314:141–145

Omrani J, Agard P, Whitechurch H, Benoit M, Prouteau G, Jolivet L (2008) Arc-magmatism and subduction history beneath the Zagros Mountains, Iran: a new report of adakites and geodynamic consequences. Lithos 106:380–398

Osterhus L, Jung S, Berndt J, Hauff F (2014) Geochronology, geochemistry and Nd, Sr and Pb isotopes of syn-orogenic granodiorites and granites (Damara orogen, Namibia)—arc-related plutonism or melting of mafic crustal sources? Lithos 200–201:386–401

Pankhurst MJ, Vernon RH, Turner SP, Schaefer BF, Foden JD (2011) Contrasting Sr and Nd isotopic behaviour during magma mingling; new insights from the Mannum A-type granite. Lithos 126:135–146

Pearce JA, Norry MJ (1979) Petrogenetic implications of Ti, Zr, Y, and Nb variations in volcanic rocks. Contrib Miner Petrol 69:33–47

Pearce JA, Harris NBW, Tindle AG (1984) Trace element discrimination diagrams for the tectonic interpretation of granitic rocks. J Petrol 25:956–983

Perugini D, Poli G, Christofides G, Eleftheriadis G (2003) Magma mixing in the Sithonia plutonic complex, Greece: evidence from mafic microgranular enclaves. Miner Petrol 78:173–200

Perugini D, Ventura G, Petrelli M, Poli G (2004) Kinematic significance of morphological structures generated by mixing of magmas: a case study from Salina Island (southern Italy). Earth Planet Sci Lett 222:1051–1066

Petford N, Atherton A (1996) Na-rich partial melts from newly underplated basaltic crust: The Cordillera Blanca Batholith, Peru. J Petrol 37:1491–1521

Philpotts AR, Shi J, Brustman C (1998) Role of plagioclase crystal chains in the differentiation of partly crystallized basaltic magma. Nature 395:343–346

Piccoli PM, Candela PA (2002) Apatite in igneous system. Rev Miner Geochem 48:255–292

Pin C, Binon M, Belin J, Barbarin B, Clemens JD (1990) Origin of microgranular enclaves in granitoids: equivocal Sr–Nd evidence from Hercynian rocks in the Massif Central (France). J Geophys Res 95:17821–17828

Piochi M, Civetta L, Orsi G (1999) Mingling in the magmatic system of Ischia (Italy) in the past 5 ka. Miner Petrol 66:227–258

Poli G (1992) Geochemistry of Tuscan Archipelago Granitoids, Central Italy: the role of hybridization processes in their genesis. J Geol 100:41–56

Poli G, Tommasini S (1990) Model for the origin and significance of microgranular enclaves in calc-alkaline granitoids. J Petrol 32:657–666

Poli G, Tommasini S, Halliday AN (1996) Trace element and isotopic exchange during acid-basic magma interaction processes. T Roy Soc Edin Earth 87:225–232

Radfar J, Amini Jehragh MR, Emami MH (1999) Geological map of Ardestan, scale 1:100000. Geological Survey of Iran, Iran

Rapp RP, Watson EB (1995) Dehydration melting of metabasalt at 8–32 kbar: implications for continental growth and crust–mantle recycling. J Petrol 36:891–931

Rezaei-Kahkhaei M, Galindo C, Pankhurst RJ, Esmaeily D (2011) Magmatic differentiation in the calc-alkaline Khalkhab–Neshveh pluton, Central Iran. J Asian Earth Sci 42:499–514

Richards JP (2015) Tectonic, magmatic, and metallogenic evolution of the Tethyan orogen: from subduction to collision. Ore Geol Rev 70:323–345

Richards JP, Spell T, Rameh E, Razique A, Fletcher T (2012) High Sr/Y magmas reflect arc maturity, high magmatic water content, and porphyry Cu ± Mo ± Au potential: examples from the Tethyan arcs of Central and Eastern Iran and Western Pakistan. Econ Geol 107:295–332

Robertson AHF (2000) Mesozoic-Tertiary tectonicsedimentary evolution of a south Tethyan oceanic basin and its margins in southern Turkey. Geol Soc Lond Spec Publ 173:97–138

Robertson A, Parlak O, Ustaömer T (2009) Melange genesis and ophiolite emplacement related to subduction of the northern margin of the Tauride? Anatolide continent, central and western Turkey. Geol Soc Lond Spec Publ 311:9–55

Rogers NW, Hawkesworth CJ, Ormerod DS (1989) Late Cenozoic basaltic magmatism in the Western Great Basin California and Nevada. J Geophys Res 100:10287–10301

Rollinson H (1993) Using geochemical data: evolution, presentation, interpretation. Longman Scientific and Technical, UK

Ross PS, Bedard JH (2009) Magmatic affinity of modern and ancient subalkaline volcanic rocks determined from trace-element discriminant diagrams. Can J Earth Sci 46:823–839

Rudnick RL, Gao S (2003) Composition of the continental crust. In: Holland HD, Turekian KK (eds) Treatise on geochemistry. Elsevier, Oxford, pp 1–64

Sadeghian M, Ghaffary M (2011) The petrogenesis of Zafarghand granitoid pluton (SE of Ardestan). Petrology 2:47–70 **(Persian with English Abstract)**

Sajona FG, Maury RC, Bellon H, Cotton J, Defant M (1996) High field strength elements of Pliocene–Pleistocene island-arc basalts Zamboanga Peninsula, Western Mindanao (Philippines). J Petrol 37:693–726

Sarjoughian F, Kananian A (2017) Zircon U-Pb geochronology and emplacement history of intrusive rocks in the Ardestan section, Central Iran. Geol Acta 15:25–36

Sarjoughian F, Kananian A, Haschke M, Ahmadian J, Ling W, Zong K (2012) Magma mingling and hybridization in the Kuh-e Dom pluton, Central Iran. J Asian Earth Sci 54–55:49–63

Saunders AD, Tarney J (1984) Geochemical characteristics of basaltic volcanism in back-arc basins. In Kokelaar BP, Howells MF (eds) Marginal basin geology: volcanic and associated sedimentary and tectonic processes in modern and ancient marginal basins, vol 16. Geol Soc London, London, pp 59–76

Schonenberger J, Marks M, Wagner T, Markl G (2006) Fluid-rock interaction in autoliths of agpaitic nepheline syenites in the Ilimaussaq intrusion, South Greenland. Lithos 91:331–351

Shafiei B, Haschke M, Shahabpour J (2009) Recycling of orogenic arc crust triggers porphyry Cu mineralization in Kerman Cenozoic arc rocks, southeastern Iran. Miner Depos 44:265–283

Sisson TW, Layne GD (1993) H_2O in basalt and basaltic andesite glass inclusions from four subduction-related volcanoes. Earth Planet Sci Lett 117:619–635

Sparks RSJ, Marshall LA (1986) Thermal and mechanical constraints on mixing between mafic and silicic magmas. J Volcanol Geoth Res 29:99–124

Sun SS, McDonough WF (1989) Chemical and isotope systematics of oceanic basalts: implications for mantle composition and processes. Geol Soc 42:313–345

Taylor SR, McLennan SM (1985) The continental crust: its composition and evolution. Blackwell Scientific Publications, Oxford

Taylor SR, McLennan SM (1995) The geochemical evolution of the continental crust. Rev Geophys 33:241–265

Thieblemont D, Tegyey M (1994) Geocchemical discrimination of differentiated magmatic rocks attesting for the variable origin and tectonic setting of calc-alkaline magmas. C R Acad Sci II 319:87–94

Vernon RH (1984) Microgranitoid enclaves: globules of hybrid magma quenched in a plutonic environment. Nature 304:438–439

Vernon RH (1990) Crystallization and hybridism in microgranitoid enclave magmas: microstructural evidence. J Geophys Res 95:17849–71859

Vernon RH (1991) Interpretation of microstructures of microgranitoid enclaves. In: Didier J, Barbarin B (eds) Enclaves and granite petrology. Elsevier, Amsterdam, pp 277–291

Vernon RH, Etheridge ME, Wall VJ (1988) Shape and microstructure of microgranitoid enclaves: indicators of magma mingling and flow. Lithos 22:1–11

Vernon RH, Johnson SE, Melis EA (2004) Emplacement-related microstructures in the margin of a deformed tonalite pluton: the San José pluton, Baja California, México. J Struct Geol 26:1845–1865

Waight TE, Maas R, Nicholls IA (2000) Fingerprinting feldspar phenocrysts using crystal isotopic composition stratigraphy: implications for crystal transfer and magma mingling in S-type granites. Contrib Miner Petrol 139:227–239

Watson EB (1982) Basalt contamination by continental crust: some experiments and models. Contrib Miner Petrol 80:73–87

Weaver BL, Tarney J (1984) Estimating the composition of the continental crust: an empirical approach. Nature 310:575–577

Weinberg RF, Sial AN, Pessoa RR (2001) Magma flow within the traverse pluton, northeastern Brazil: compositional and thermal convection. Geol Soc Am Bull 113:508–520

White AJR, Chappell BW (1977) Ultrametamorphism and granitoid genesis. Tectonophysics 43:7–22

White AJR, Chappell BW, Wyborn D (1999) Application of the restite model to the Deddick Granodiorite and its enclaves—a reinterpretation of the observations and data of Maas et al. (1997). J Petrol 40:413–421

Whitechurch H, Omrani J, Agard P, Humbert F, Montigny R, Jolivet L (2013) Evidence for Paleocene–Eocene evolution of the foot of the Eurasian margin (Kermanshah ophiolite, SW Iran) from back-arc to arc: implications for regional geodynamics and obduction. Lithos 182–183:11–32

Wu FY, Jahn BM, Lin Q (1998) Isotopic characteristics of the post-orogenic granite in orogenic belt of northern China and their implications in crustal growth. Chin Sci Bull 43:420–424

Wu FY, Jahn BM, Wilde SA, Sun DY (2000) Phanerozoic crustal growth: U-Pb and Sr-Nd isotopic evidence from the granites in northeastern China. Tectonophysics 328:89–113

Wu RX, Zheng YF, Wu YB, Zhao ZF, Zhang SB, Liu X, Wu FY (2006) Reworking of juvenile crust: element and isotope evidence from Neoproterozoic granodiorite in South China. Precambrian Res 146:179–212

Yang JH, Wu FY, Wilde S, Xie LW, Yang YH, Liu XM (2007) Tracing magma mixing in granite genesis: in situ U–Pb dating and Hf-isotope analysis of zircons. Contrib Miner Petrol 153:177–190

Yang XM, Lentz DR, Chi G, Thorne KG (2008) Geochemical characteristics of gold-related granitoids in southwestern New Brunswick, Canada. Lithos 104:355–377

Yang YH, Zhang HF, Chu ZY, Xie LW, Wu FY (2010) Combined chemical separation of Lu, Hf, Rb, Sr, Sm and Nd from a single rock digest and precise and accurate isotope determinations of Lu–Hf, Rb–Sr and Sm–Nd isotope systems using Multi-Collector ICP-MS and TIMS. Int J Mass Spectrom 290:120–126

Yang H, Ge WC, Zhao GC, Dong Y, Xu WL, Ji Z, Yu JJ (2015a) Late Triassic intrusive complex in the Jidong region, Jiamusi–Khanka Block, NE China: Geochemistry, zircon U–Pb ages, Lu–Hf isotopes, and implications for magma mingling and mixing. Lithos 224–225:143–159

Yang LQ, Deng J, Qiu KF, Ji XZ, Santosh M, Song KR, Song YH, Geng JZ, Zhang C, Hua B (2015b) Magma mixing and crust–mantle interaction in the Triassic monzogranites of Bikou Terrane, central China: Constraints from petrology, geochemistry, and zircon U–Pb–Hf isotopic systematics. J Asian Earth Sci 98:320–341

Yilmaz Sahin S (2008) Geochemistry of mafic microgranular enclaves in the Tamdere Quartz Monzonite, south of Dereli/Giresun, Eastern Pontides, Turkey. Chem Erde Geochem 68:81–92

Zhang Y, Ni H, Chen Y (2010) Diffusion data in silicate melts. Rev Miner Geochem 72:311–408

Zhang X, Yuan L, Wilde SA (2014a) Crust/mantle interaction during the construction of an extensional magmatic dome: middle to Late Jurassic plutonic complex from western Liaoning, North China Craton. Lithos 205:185–207

Zhang J, Ma C, Xiong F, Liu B, Li J, Pan Y (2014b) Early Paleozoic high-Mg diorite-granodiorite in the eastern Kunlun Orogen, western China: response to continental collision and slab break-off. Lithos 210–211:129–146

Zhang Y, Sun M, Yuan C, Xu Y, Long X, Tomurhuu D, Wang CY, He B (2015) Magma mixing origin for high Ba–Sr granitic pluton in the Bayankhongor area, central Mongolia: response to slab roll-back. J Asian Earth Sci 113:353–368